Heat Transfer Through Grass: A Numerical Application

MSc Thesis

Sabine van Dijk

Delft University of Technology

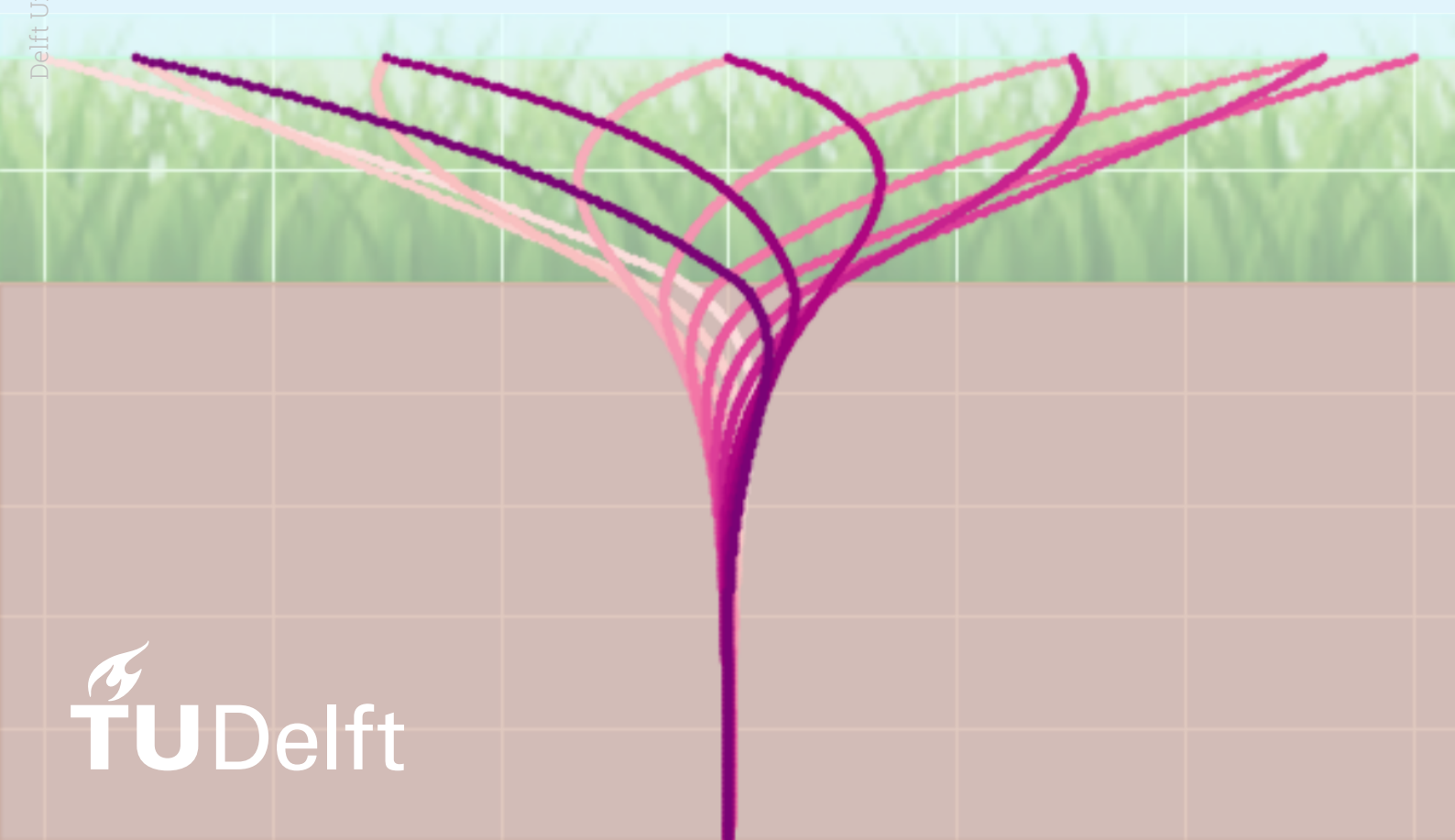

TU Delft

Heat Transfer Through Grass: A Numerical Application

by

Sabine van Dijk

to obtain the degree of Master of Science
at the Delft University of Technology,
to be defended publicly on Tuesday February 18, 2025 at 15:00 PM.

Student Number:	4965469	
Thesis Committee:	Prof. dr. ir. B.J.H. van de Wiel	TU Delft, Supervisor
	Dr. ir. S.J.A. van der Linden	TU Delft, Supervisor
	Dr. ir. M. Rohde	TU Delft, Faculty of App. Sci.
Project Duration:	May, 2024 - February, 2025	
Faculty:	Faculty of Applied Sciences, TU Delft	

Cover: Numerical model for a two-layer diffusive system without sources, with a cosine signal at the top boundary.

TU Delft

Abstract

Accurate modelling of soil and grass temperatures is essential for improving weather prediction models. The soil and grass temperatures are used to determine the surface temperature, which is a key parameter in latent and sensible heat flux calculations.

The surface temperature is often estimated using land surface parametrisation schemes, such as empirical skin resistance models. These parametrisations often lead to deviations and temporal shifts in the heat flux at the surface, causing a discrepancy in the closure of the surface energy balance (SEB) on short time scales. Addressing these inconsistencies requires a more refined approach to model heat transfer processes within the vegetation-soil continuum.

This research investigates the accuracy of a two-layer diffusive model with uniform thermal parameters in capturing temperature dynamics within the vegetation-soil continuum. The results indicate that a purely diffusive model accurately describes temperature dynamics within the soil. However, this approach is too simplistic to capture the complexity of heat transfer within the vegetation layer. Within the soil, the thermal diffusivity (κ_{soil}) remains relatively constant over time. An optimal value is determined as $\kappa_{soil} = 3.0 \pm 0.3 \cdot 10^{-7}$ m^2 s^{-1}, in line with values reported in previous research. In contrast, heat transfer within the grass is influenced by additional processes beyond pure diffusion. Preliminary analysis shows an improvement in the model performance with the introduction of a linear source term, likely accounting for radiative effects.

A diffusive approach to in-canopy heat transfer, combined with a source term, presents a promising step in describing the vegetation layer in surface heat transfer models. However, further research is necessary to refine the formulation of the source term, whether through a physically motivated or data-driven approach.

From a broader perspective, further additional observational and numerical research into the physical processes behind heat transfer within the grass layer is advised to assess their influence. Additionally, generalisation of the model will enhance its applicability in weather forecasting models to improve the prediction of thermal effects near the surface.

Contents

1

Introduction

Accurate determination of both grass and soil temperature are essential for weather forecasting and climate simulation models. These temperatures play a key role in calculating components of the surface energy balance (SEB), which governs the exchange of energy between the land surface and the atmosphere. The SEB ensures that all energy fluxes at the surface add up to zero [1, 2]. In general, the SEB is composed of four energy fluxes; net radiation, sensible heat flux, latent heat fluxes (evapotranspiration) and conductive heat flux into the ground. These components are often not measured directly. Instead, they are calculated with models that use the surface temperature as an input parameter [3].

The surface temperature is often inferred rather than directly measured. Observations are usually taken at different heights, such as air temperature above the canopy or soil temperature a few centimetres below the surface. Since these measurements are vertically displaced from the surface, models must be used to extrapolate the temperatures and heat fluxes to the surface. The use of models introduces uncertainties, especially in how heat is transferred through vegetation layers such as grass.

Soil heat transfer has been extensively studied as a diffusive process using Fourier analysis [4, 5, 6]. This method provides reasonable accuracy for calculating the soil heat flux. Modelling in-canopy temperature dynamics, however, remains a challenge, despite its importance. This is due to the complexity of heat transfer processes within vegetation. Short vegetation layers, such as grass, have traditionally been simplified using empirical parametrisations, such as skin resistance models [7].

This is due to computational limitations, but more importantly to the fact that accurate observational validation data is often unavailable. These empirical approaches often fail to capture the dynamic, frequency-dependent nature of heat transfer through vegetation layers, especially on short time scales [8].

Recent studies have demonstrated that vegetation influences both the amplitude and phase of temperature fluctuations in the underlying soil [9]. Short-term temperature variations, such as those caused by varying cloud cover, primarily affect the upper vegetation layers. Longer-term variations, such as diurnal cycles, propagate through the entire vegetation layer and into the soil. Capturing both high- and low frequency effects is critical for accurately predicting temperature profiles and heat fluxes in vegetated environments.

Under the assumption that vegetation can be regarded as a homogeneous diffusive medium with distinct thermal diffusivity and conductivity, a numerical two-layer model has been developed. This model applies harmonic analysis to model temperature profiles and heat fluxes through the combined grass and soil layers. Initial results by Linden et al. [9] show promise in predicting surface heat fluxes, as well as in achieving better closure of the surface energy balance. Here, the effective interface for evaluation of the SEB was placed at the top of the vegetation [9]. However, the assumptions and parameters of the analytical model require further validation, particularly when applied to observational data.

A major advancement in this study is the use of newly available high-resolution in-canopy temperature measurements. Until recently, it was not possible to evaluate the thermal properties of the canopy this

closely. For small canopies, the vertical resolution of in-canopy measurements was too low to investigate the temperature profiles in depth. However, the development of a new measurement method by Horst [10], has enabled millimetre resolution temperature profiles to be obtained for the first time. High-resolution temperature observations inside the grass allow us to extend the validation of the diffusion model.

The research question is as follows: How well does a purely diffusive model describe temperature dynamics in soil and vegetation layers, and what additional processes must be considered to improve its accuracy within these layers?

To answer this research question the study of heat transfer through vegetation and soil is extended with a numerical model. Specifically, the aim is to:

- Verify the accuracy of the numerical two-layer diffusive model by comparing it with the analytical solution.
- Compare modelled temperature profiles with high-resolution field data to evaluate the model's applicability to the vegetation and soil layers and determine the optimal thermal diffusivities for both layers.
- Investigate potential adjustments to the model to address discrepancies and improve accuracy in predicting temperature profiles and heat fluxes.

First, Chapter 2 describes the theory of heat transfer and presents the analytical solution to the diffusion problem. Next, the numerical model and analysis methods are introduced. In Chapter 4 the results are presented, showing the accuracy of the numerical model and evaluating the model's applicability by comparing the model's temperature profiles to the soil and vegetation data. Chapter 5 presents an adjustment to the model that incorporates an additional source term, presumably accounting for the radiative effects. Chapter 6 discusses the findings along with recommendations for future research, concluding with Chapter 7 summarising the findings of the research question.

2

Theory

This chapter provides an overview of the physics underlying the numerical model. Modelling temperature profiles in the vegetation-soil continuum requires a thorough understanding of heat transfer. Based on the principles of heat transfer, the governing equations for the two-layer system are derived. The chapter then introduces the harmonic method, which is employed to solve the governing equations. Finally, the analytical solution for the temperature profile within the homogeneous two-layer system is derived. This analytical solution will be used as a benchmark for the numerical model.

2.1. Heat Transfer

Heat transfer governs the distribution of internal energy within and between materials. Analysing the mechanisms of heat transfer provides the mathematical framework necessary to model temperature profiles in the vegetation-soil continuum. Heat fluxes at boundaries describe the energy exchange between media and directly determine the boundary conditions at their interface.

Heat transfer occurs through one or more of three fundamental mechanisms: conduction, convection, and radiation [11].

Conduction, the first fundamental mechanism, is heat transfer through direct molecular interaction within a medium. Conductive heat transfer is driven by a temperature gradient and depends on the thermal properties of the medium. Thermal conductivity, λ, is a measure of the ability of a material to conduct heat. Fourier's law of heat conduction relates the thermal conductivity and the temperature gradient to the heat flux, $\mathbf{q}$ [W m^{-2}] [12]:

$$\mathbf{q} = -\lambda \nabla T, \tag{2.1}$$

where λ [W m^{-1} K^{-1}] is the thermal conductivity of the medium. The negative sign indicates that the heat flux is opposite in direction to the temperature gradient, meaning heat flows from regions of higher temperature to lower temperature.

Convection, the second fundamental mechanism, is the transport of energy by the occurrence of fluid flow [12]. For instance, the air between the blades of grass can facilitate this form of heat transfer. In contrast, the solid grass and soil layers are incapable of convective heat transfer.

The third form of heat transfer is *radiation*. Radiative heat transfer is an electromagnetic mechanism, that transports energy with the speed of light and needs no medium [12]. The Stefan-Boltzmann law describes the total radiative heat flux emitted by a surface across all wavelengths. In the context of the Earth's surface, thermal radiation is predominantly emitted in the longwave infrared spectrum. The radiant heat flow between two media, $\mathbf{q}_{rad}$ [W m^{-2}], is given by:

$$\mathbf{q}_{rad} = \sigma \left(\varepsilon_1 T_1^4 - \varepsilon_2 T_2^4 \right), \tag{2.2}$$

where σ, the Stefan-Boltzmann constant, the constant of proportionality with a value of $\sigma = 5.67 \cdot 10^{-8}$ W m^{-2} K^{-4}. T_1 and T_2 are the temperatures [K] of the two media, and ε_1 and ε_2 denote the emissivity [-] of each surface.

Having introduced the mechanisms of heat transfer, attention is now directed to the temperature distribution within media. Since the temperature distribution is intrinsically linked to the energy distribution, the temperature dynamics inside the medium can be analysed through a differential equation that describes the local energy balance.

The energy balance equation describes the change of energy, incorporating all processes that contribute to energy changes. For a given control volume, the total energy balance is expressed as:

$$\rho c_p \left(\frac{\partial T}{\partial t} + \mathbf{v} \cdot \nabla T \right) = \Phi - \nabla \cdot \mathbf{q} + S, \tag{2.3}$$

where on the left-hand side ρ [kg m^{-3}] is the density, c_v [J kg^{-1} K^{-1}] is the specific heat capacity at constant pressure, and $\mathbf{v}$ [m s^{-1}] is the velocity vector within the control volume. On the right-hand side, Φ is the viscous dissipation term, $\nabla \cdot \mathbf{q}$ is the divergence of the heat flux, and S represents a source or sink term for the energy generated within the volume, all in units of [W m^{-3}].

At the start of this thesis, the following assumptions are made, in line with the diffusive approach by Linden et al. [9]:

1. **Dominant conductive heat transfer:** It is assumed that heat transfer occurs predominantly through conduction within the grass-soil continuum. Convection and radiation are considered negligible compared to conductive heat transfer, implying that both wind and radiation do not penetrate the top of the vegetation. This assumption allows for the simplification of the energy balance by considering only the divergence of the conductive heat flux.
2. **Homogeneity:** It is assumed that both the grass layer (denoted as $j = veg$) and the soil layer ($j = soil$) are homogeneous. This implies that the thermal properties, λ, c_v and ρ are constant with depth for both media.
3. **1D model:** It is assumed that there are no horizontal gradients in the temperature distribution, i.e., $\frac{\partial}{\partial x} = \frac{\partial}{\partial y} = 0$.
4. **No energy sources or sinks:** It is assumed that there are no internal energy sources or sinks within the two media, i.e., $S = 0$. (Note: This assumption is released at the end of this thesis.)

In reality, the grass and soil are not exactly homogeneous media. The soil is composed of a combination of namely clay, water and organic material, each with different conductive properties. Under real-world conditions, the conductive properties of the soil can be irregular in height depending on the composition of materials, and can even be irregular in time due to fluctuations in soil moisture [13].

Likewise, the grass layer consists of a composite of grass and air. Moreover, the grass is more dense near the ground, creating a non-homogeneous distribution in density. The fact that the top is less dense makes it also easier for air to flow through. Convective heat transport may then become important. Nevertheless, the reality is simplified by assuming that the grass-air layer is some form of a homogeneous 'sponge' with uniform conductive properties.

The third assumption neglects energy sources and sinks from condensation or evaporation. It also neglects an energy source from incoming solar radiation. With the assumption that grass is a homogeneous medium, we choose an average top of the grass. All energy from radiation is assumed to be absorbed and/or emitted at or above this top.

The simplified model is depicted in Figure 2.1. The red dashed line shows that an average grass height is taken to be the radiative top of the now homogeneous grass layer. For convenience, the direction of the z-axis is defined positive downward with $z = 0$ m located at the top of the grass layer (red dashed line).

Within the homogeneous media, the 'sponge-like' grass and solid soil layers, there is no bulk velocity ($\mathbf{v} = 0$) and there is no viscous dissipation ($\Phi = 0$). Combining this with the above assumptions, Equation 2.3 can be rewritten as the following governing equation for the system:

$$\frac{\partial T_j}{\partial t} = \frac{\lambda_j}{\rho_j c_j} \frac{\partial^2 T_j}{\partial z^2} = \kappa_j \frac{\partial^2 T_j}{\partial z^2}, \tag{2.4}$$

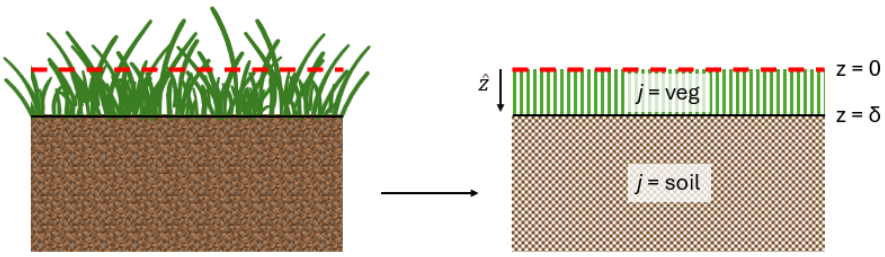

Figure 2.1: Simplified model of the grass-soil continuum. Where in reality (left) soil and grass layers are non-homogeneous, the model (right) assumes two homogeneous layers. The red dashed line is the top of the grass in the model, under which energy production is assumed to be zero.

where κ_j [m^2 s^{-1}] is the thermal diffusivity in layer j.

The simplified heat flux in each layer becomes

$$q_j(z,t) = -\lambda_j \frac{\partial T_j}{\partial z}. \tag{2.5}$$

2.2. Harmonic Method

A common way to solve for the temperature profile within a medium is with the *harmonic method* (see, e.g., [14, 15, 4]). It uses the superposition principle, by assuming that the general solution to Equation 2.4 is given as a sum of cosines. The harmonic method uses this sum of cosines, i.e., a Fourier series, to mathematically describe the temperature at different heights. The solution is of the following form:

$$T_j(z,t) = \bar{T} + \sum_n A_n(z) cos(\omega_n t + \phi_n(z)), \tag{2.6}$$

where $\bar{T}$ is the temperature at infinite depth, and ω_n is n^{th} frequency in the Fourier series. The amplitude, $A_n(z)$, and phase, $\phi_n(z)$, depend on both the frequency (ω_n) and the depth (z).

For amplitude, the dependency is given by the following equation:

$$A_n(z) = A_n(0) \cdot \mathrm{e}^{-z/D_j}, \tag{2.7}$$

where D_j[m] is the damping depth (also known as e-folding depth) and is given as:

$$D_j \equiv \sqrt{\frac{2\kappa_j}{\omega_n}}. \tag{2.8}$$

Note that the ω_n makes the value of D_j frequency dependent, and the κ_j shows that the damping depth is dependent on the medium.

The depth dependence of the phase is as follows:

$$\phi_n(z) \equiv \phi_n(0) - z/D_j, \tag{2.9}$$

From this, the properties of the solution can be deduced. For example, the phase shift of the each frequency component decreases linearly with depth, $-z/D_j$. This is in line with the expected delay of the signal at greater depths.

2.3. Analytical Solution to the Two-Layer Problem

The analytical solution to the governing equations (Eq. 2.4 and Eq.2.5) has been derived by Linden et al. [9]. Below, an overview of the main steps leading to the final solution is provided. As illustrated in Figure 2.1, the vertical coordinate $z = 0$ is defined at the top of the vegetation layer, while the interface between the two layers is located at $z = \delta$.

To solve the problem for each frequency ω, the following boundary conditions are imposed:

$$T_{veg}(0,t) = \bar{T} + A\cos(\omega t) = \frac{A}{2}\left(\mathrm{e}^{\mathrm{i}\omega t} + \mathrm{e}^{-\mathrm{i}\omega t}\right), \tag{2.10a}$$

$$T_{veg}(\delta,t) = T_{soil}(\delta,t), \tag{2.10b}$$

$$\lambda_{veg}\frac{\partial T_{veg}}{\partial z}\bigg|_{z=\delta} = \lambda_{soil}\frac{\partial T_{soil}}{\partial z}\bigg|_{z=\delta} \quad ;\forall t, \tag{2.10c}$$

$$\lim_{z\to\infty} T_{soil}(z,t) = \bar{T} = 0, \tag{2.10d}$$

At the top of the vegetation layer, a cosine temperature profile is applied (Eq. 2.10a), representing a time-periodic fluctuation with amplitude A and frequency ω. Continuity of temperature at the interface between the vegetation and soil ($z = \delta$) is ensured by boundary condition 2.10b. The third condition, 2.10c enforces continuity of heat flux, accounting for differences in thermal conductivity (λ) between the layers. Lastly, deep inside the soil ($z \to \infty$) the temperature approaches a mean value $\bar{T}$, which is set to zero for simplicity.

This choice is justified by the linearity of the heat equation. Since temperature variations are of primary interest, subtracting a constant mean value simplifies the equations without affecting the behaviour of the solution. Mathematically, the temperature can be expressed as the sum of a steady mean component and a fluctuating part. Since $\bar{T}$ is zero its time derivative is zero, as well as its spatial derivatives. This ensures that removing $\bar{T}$ does not influence the behaviour of the fluctuating temperature field. If the actual mean temperature is non-zero, it can be reintroduced by adding a constant shift to the final solution.

Since the temperature at the top boundary oscillates as a cosine function with frequency ω, the temperature at any depth in the grass and subsequently in the soil must also oscillate at this same frequency. However, as the thermal wave propagates, it undergoes both attenuation and a phase shift. This leads to the Ansatz:

$$T_j(z,t) = A_j(z)cos(\omega t + \phi_j(z)), \tag{2.11}$$

where $A_j(z)$ represents the amplitude and $\phi_j(z)$ the phase shift of the temperature variation, both of which depend on depth. This Ansatz facilitates the solution process by transforming the governing partial differential equation (PDE) into an ordinary differential equation (ODE).

By applying the governing equations, boundary conditions and Ansatz, the following analytical solutions were derived by Linden et al. [9]:

$$\begin{aligned} T_{veg}(z,t) =& \frac{A}{2}\left(\frac{e^{-\beta_{veg}z} - e^{\beta_{veg}z}}{1+\left(\frac{m-1}{m+1}\right)e^{-2\beta_{veg}\delta}} + e^{\beta_{veg}z}\right)e^{\mathbf{i}\omega t} \\ &+\frac{A}{2}\left(\frac{e^{-\beta^*_{veg}z} - e^{\beta^*_{veg}z}}{1+\left(\frac{m-1}{m+1}\right)e^{-2\beta^*_{veg}\delta}} + e^{\beta^*_{veg}z}\right)e^{-\mathbf{i}\omega t}, \end{aligned} \tag{2.12}$$

$$\begin{aligned} T_{soil}(z,t) =& \frac{A}{2}\left(\frac{e^{-\beta_{veg}\delta} - e^{\beta_{veg}\delta}}{1+\left(\frac{m-1}{m+1}\right)e^{-2\beta_{veg}\delta}} + e^{\beta_{veg}z}\right)\frac{e^{-\beta_{soil}z}}{e^{-\beta_{soil}\delta}}e^{\mathbf{i}\omega t} \\ &+\frac{A}{2}\left(\frac{e^{-\beta^*_{veg}\delta} - e^{\beta^*_{veg}\delta}}{1+\left(\frac{m-1}{m+1}\right)e^{-2\beta^*_{veg}\delta}} + e^{\beta^*_{veg}z}\right)\frac{e^{-\beta^*_{soil}z}}{e^{-\beta^*_{soil}\delta}}e^{-\mathbf{i}\omega t}, \end{aligned} \tag{2.13}$$

where $\beta_j = \sqrt{\omega/(2\kappa_j)}(1+\mathbf{i})$, and $m = (\lambda_{veg}/\lambda_{soil})\sqrt{\kappa_{soil}/\kappa_{veg}}$ is the ratio between the thermal conductivities and diffusivities of the two layers. This solution for the temperature profiles within the two media is used to validate the numerical model.

3

Numerical Method

To accurately model the temperature distribution within the vegetation-soil layer, the thermal properties of both vegetation and soil must be precisely determined. Since these thermal properties can vary significantly across different sites and conditions [13], a numerical model offers a flexible and efficient approach to adapt to such variations. Moreover, closed-form analytical solutions for equations with time-dependent variables are often not available, highlighting the need for a numerical approach.

In the previous chapter, an analytical solution was derived for the temperature distribution within the vegetation and soil layers, based on a set of simplifying assumptions discussed in Section 2.1. This chapter describes the discretisation of the heat equation, forming the basis for our numerical model. Special attention is given to the vegetation-soil interface, where the temperature must be continuous despite the discontinuity in thermal properties when going from the vegetation to the soil layer. Subsequently, the criterion for numerical stability is analysed, showing how explicit numerical models require a fine grid resolution to remain stable. This criterion serves as a guideline to decide on the temporal and spatial discretization, i.e., the numerical grid. Finally, the method for model validation and thermal property estimation is explained. Validation is performed on a two-layer model, while thermal properties are determined with a decoupled model. The relationship between the coupled and decoupled models is clarified to show how thermal properties are inferred.

3.1. Discretisation of the Heat Equation

The discretisation is performed using the method described in Chapter 6 of *Modelling Physical Transport Phenomena* by K.Hanjalic et al. [16]. Specifically, the finite difference method (FDM) used is the FTCS (Forward in Time, Central in Space) scheme. The FTCS method is convenient as it relies only on values (already known) from the previous time step. However, being explicit, this finite difference method comes with strict requirements for grid refinement to ensure numerical stability. These stability criteria are discussed in a later section.

Applying the FTCS method, the heat equation (Eq. 2.4) is discretised as follows:

$$\frac{T[k,i]-T[k,i-1]}{\Delta t}=\kappa_j\left(\frac{T[k-1,i-1]-2\cdot T[k,i-1]+T[k+1,i-1]}{\Delta z^2}\right), \tag{3.1}$$

where Δt is the temporal and Δz is the spatial grid spacing. The time step index is indicated by i, and k gives the spatial grid point index.

The equation can be rewritten for the temperature in time step, i, and at location k, $T[k,i]$:

$$T[k,i]=T[k,i-1]+\left(\frac{\kappa_j\Delta t}{\Delta z^2}\right)\left(T[k-1,i-1]-2\cdot T[k,i-1]+T[k+1,i-1]\right). \tag{3.2}$$

We can regroup the terms on the right-hand side to:

$$T[k,i] = \left(1 - 2\left(\frac{\kappa_j \Delta t}{\Delta z^2}\right)\right) T[k,i-1] + \left(\frac{\kappa_j \Delta t}{\Delta z^2}\right) T[k-1,i-1] + \left(\frac{\kappa_j \Delta t}{\Delta z^2}\right) T[k+1,i-1]. \tag{3.3}$$

Now we can calculate the temperature $T[k,i]$ using the temperatures at the previous time step, $i-1$, at the same and neighbouring sites.

3.2. Temperature at the Interface

When transitioning from the vegetation layer to the soil layer, there is a discontinuity in thermal properties, e.g., thermal diffusivity κ. Despite this, the temperature must be continuous at the vegetation-soil interface. The discontinuity poses a challenge when computing the interface temperature using Equation 3.2, which requires the thermal diffusivity at the calculated location. Since thermal diffusivity is undefined *at* the interface, an alternative approach is needed. One that relies only on the thermal properties of neighbouring cells rather than the interface itself.

The solution is derived from the flux equation 2.5 and the boundary condition at the interface 2.10c, which ensures energy conservation by requiring that heat fluxes on both sides of the interface are in balance.

This interface condition is discretised to:

$$\lambda_{veg} \cdot \frac{T[k_{interface},i] - T[k_{interface}-1,i]}{\Delta z} = \lambda_{soil} \cdot \frac{T[k_{interface}+1,i] - T[k_{interface},i]}{\Delta z}, \tag{3.4}$$

where λ_{veg} and λ_{soil} are the thermal conductivities of vegetation and soil respectively, and $T[k_{interface},i]$ represents the temperature at the interface at time step i.

Rearranging this equation to solve for the temperature $T[k_{interface},i]$ gives:

$$T[k_{interface},i] = \frac{(\lambda_{veg} \cdot T[k_{interface}-1,i] + \lambda_{soil} \cdot T[k_{interface}+1,i])}{(\lambda_{veg} + \lambda_{soil})}. \tag{3.5}$$

3.3. Numerical Stability

For the numerical solution to show physically realistic behaviour and remain balanced everywhere (i.e. not diverge), stability conditions must be satisfied. According to the book *Modelling Physical Transport Phenomena* by K. Hanjalic [16], four basic rules should be followed to ensure numerical stability. Three of these rules are inherently satisfied for the situation studied here. The fourth one, which requires that all coefficients of the discretised equation must always be positive, needs to be checked. This rule ensures that an increase in temperature at one grid point leads to increases in neighbouring grid points.

We know that the term $\left(\frac{\kappa \Delta t}{\Delta z^2}\right)$ is inherently positive, so no further investigation is required. The critical term is the coefficient of $T[k,i-1]$. To ensure this term remains positive, the following condition must hold:

$$1 - 2\left(\frac{\kappa \Delta t}{\Delta z^2}\right) > 0. \tag{3.6}$$

Rearranging this gives the stability criterion:

$$\left(\frac{\kappa \Delta t}{\Delta z^2}\right) < \frac{1}{2}. \tag{3.7}$$

If this condition is violated, physically unrealistic results can be obtained. A consequence of this stability criterion for explicit schemes is that, when Δz is refined to improve spatial accuracy, then significantly smaller time steps Δt are required. This results in increased computational costs.

3.4. Implementation Method

To solve the heat equation numerically, the computational grid must be carefully defined, and the initial and boundary conditions must be set appropriately. These conditions depend on the grid resolution, which is constrained by the stability criterion discussed earlier (see Equation 3.7). This section describes the process of defining the computational grid and preparing the initial and boundary conditions for model validation.

3.4.1. Three Used Models

In this research, three models are used to evaluate the vegetation-soil continuum. These three models are depicted in Figure 3.1.

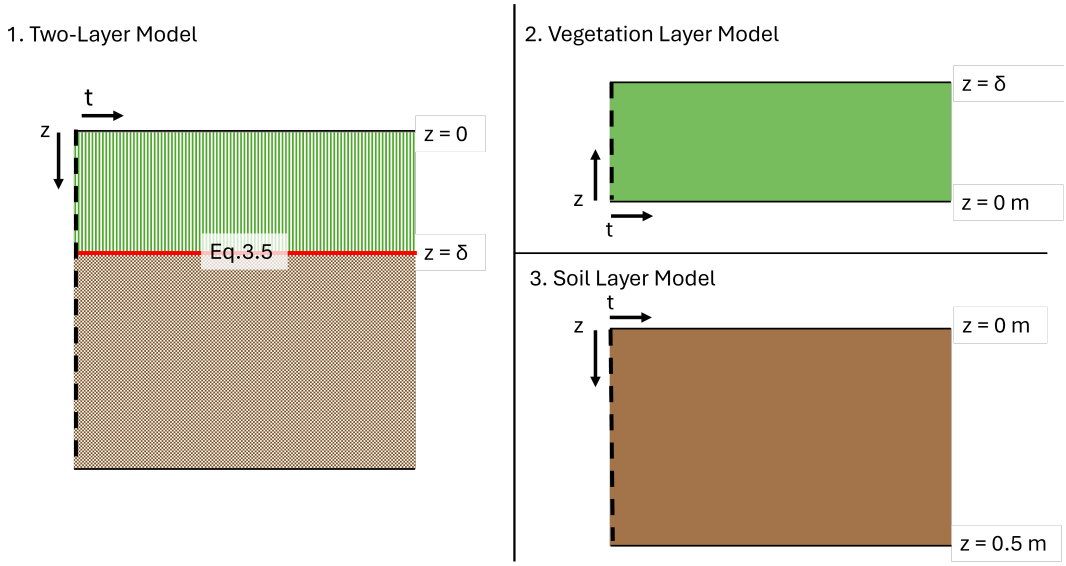

Figure 3.1: Schematic presentation of the three models used in this study, shown in 2D with spatial (z) and temporal (t) dimensions. The black dotted line represents the initial condition, whereas the normal black lines indicate the boundary conditions. The red line marks the interface, where the temperature is computed using Eq. 3.4. In this research the canopy height is set to δ = 0.2 m.

For the Two-Layer Model, shown on the left-hand side, the z-direction is positive downward, starting from $z = 0$ at the top of the vegetation layer. The Soil-Layer Model follows the same convention, with $z = 0$ m at the surface and extending to $z = 0.5$ m at the bottom, corresponding to the observation depths. In contrast, the Vegetation-Layer Model, defines the z-direction as positive upward, with the ground surface at $z = 0$ m and the top of the canopy at $z = \delta = 0.2$ m.

Within each model Equation 3.2 is used for the computation of temperature within the layers. For the Two-Layer Model, which has an interface between the media, Equation 3.5 is applied to calculate the temperature at the interface (red line).

The boundary conditions are depicted as black lines, while the initial condition is shown as a black dotted line for all three models.

3.4.2. Grid Resolution

The resolution of the computational grid is important for ensuring numerical stability and achieving accurate results. The spatial step size Δz is related to the temporal step size Δt by the stability condition, Eq. 3.7. The resolutions chosen for the three different models are elaborated below.

For the two-layer model, the time resolution is chosen to have a value of $\Delta t = 1$ second. The spatial resolution Δz is the smallest value that satisfies the stability criterion. Using typical values for the thermal diffusivity, $\kappa_{veg} = 12 \cdot 10^{-7}$m^2 s^{-1}, $\kappa_{soil} = 3 \cdot 10^{-7}$m^2 s^{-1} as found in previous research [9], the

minimal Δz for which the stability criterion is satisfied in both layers is:

$$\Delta z = \sqrt{2\kappa_{veg}\Delta t} = 1.55 \text{ mm}. \tag{3.8}$$

For the soil layer model, the same time resolution of $\Delta t = 1$ second is chosen. The spatial resolution is chosen at $\Delta z = 2.5$ mm, fulfilling the stability criterion and ensuring high accuracy. This grid resolution allows for κ_{soil} to be evaluated up to $3.12 \cdot 10^{-6}$m^2 s^{-1}.

For the vegetation layer model, the numerical step size is conveniently selected to match the observational step size, Δz = 1.25 mm. For Δt = 1 second this only satisfies the criterion for $\kappa_{veg} \leq 7.8 \cdot 10^{-7}$m^2 s^{-1}. To investigate κ_{veg} around the expected value of $12 \cdot 10^{-7}$m^2 s^{-1}, a finer time resolution is used, $\Delta t = 1/4$ second. This allows κ_{veg} to be evaluated up to $3.12 \cdot 10^{-6}$m^2 s^{-1}.

Summary of Grid Parameters

The grid resolutions for the different models are summarized in Table 3.1. For the two-layer model the thermal parameters used are the optimal thermal properties found in previous research (see, [9]). In the decoupled models for both the soil and the vegetation κ is evaluated up to a value of $3.12 \cdot 10^{-6}$ m^2 s^{-1}, and the thermal conductivity (λ) is not used in these one layer models.

Table 3.1: Grid parameters and thermal parameters in different models.

Model Type	Δt (s)	Δz (mm)	κ (m^2 s^{-1})	λ (W m^{-1}K^{-1})
Two-Layer Model	1	1.55	$\kappa_{\text{veg}} = 12 \cdot 10^{-7}$, $\kappa_{\text{soil}} = 3 \cdot 10^{-7}$	$\lambda_{veg} = 0.44$, $\lambda_{soil} = 0.52$
Soil Layer Model	1	2.5	up to $3.12 \cdot 10^{-6}$	x
Vegetation Layer Model	0.25	1.25	up to $3.12 \cdot 10^{-6}$	x

3.4.3. Initial and Boundary Conditions

With the computational grid defined, the final step before solving the numerical model is to set the initial and boundary conditions. These conditions differ for each of the three models.

Two-Layer Model

The two-layer model is used for validation against the analytical solution. To ensure consistency, the boundary and initial conditions are chosen to match the analytical solution. The initial temperature profile, $T[k, 0]$, is imposed using the analytical solution.

- Within the vegetation layer ($k < k_{interface}$), the initial temperature is given by Equation 2.12.
- Within the soil layer ($k \geq k_{interface}$), it is determined by Equation 2.13.

The top boundary condition follows a prescribed diurnal temperature variation:

$$T[0, i] = A \cdot \cos(\omega_{day} t[i]) + \bar{T}, \tag{3.9}$$

where ω_{day} [s^{-1}] is the diurnal frequency, $A = 3$°C is the amplitude, and $\bar{T} = 15$°C is the prescribed mean temperature. The bottom boundary condition is a constant prescribed temperature for all time steps, $\bar{T} = 15$°C.

Decoupled Soil and Vegetation Layer Models

The soil and vegetation layer models are used to compare numerical results with observed data. Therefore, their initial and boundary conditions are derived from the observational data within these media.

For the initial condition, the observed temperature profile is interpolated *over height* using Spline interpolation to match the spatial grid resolution of the model. However, for the vegetation layer model, the spatial grid resolution is already aligned with the vertical resolution of the observations, so height interpolation is unnecessary.

For the boundary conditions, the observed temperature data is interpolated *in time* using Spline interpolation to match the temporal resolution of the model. Observations are recorded at $\Delta t = 5$ sec for vegetation and $\Delta t = 10$ min for the soil, while the model operates with a temporal resolution of $\Delta t = 1$ second.

With the grid and boundary conditions defined, the numerical models can now be used. The two-layer model is validated against the analytical solution, while the soil and vegetation layer models generate temperature profiles for comparison with observations. This comparison is the basis for optimising the thermal parameters discussed in the next section.

3.5. Determining Thermal Parameters

In order to determine the optimal thermal properties for the soil and the vegetation, the following steps are executed:

1. The numerical model is executed for a value of κ_j between 0 and $3.12 \cdot 10^{-6}$m^2 s^{-1}. This way temperature solutions at all grid points in space and in time are generated.
2. The modeled temperatures at the depths and times corresponding to the measured profiles are extracted for comparison with the observations.
3. The Root Mean Squared Error (RMSE) is calculated as follows:

$$RMSE = \sqrt{\frac{1}{N_t N_x} \sum_{i=0}^{N_t} \sum_{k=0}^{N_z} \left(T_{modeled,\kappa_j}[k,i] - T_{observed}(z_k, t_i) \right)^2}, \tag{3.10}$$

   where N_t and N_z represent the number of observed data points in the selected time and space, respectively. The RMSE quantifies the discrepance between the modeled temperature profiles for a certain κ_j and the observed temperatures.
4. The process is repeated for different values of κ_j till a minimum value for the RMSE is found. This minimum RMSE indicates the best estimate for the thermal diffusivity, κ_j.

In this research, the optimal value for κ_j is determined daily, since thermal diffusivity can vary over time due to moisture and density fluctuations.

With the model setup and evaluation method defined, the next chapter continues with the validation of the numerical model and the analysis of the results.

4

Model Validation and Results

This chapter presents the results obtained from the validation and application of the numerical model developed in this study. The results are divided into two main sections. First, the performance of the two-layer model is evaluated by comparing its numerical results with the analytical solution. This step is crucial to ensure the model's accuracy and reliability.

Second, the two-layer model is decomposed into two one-layer models to investigate the thermal diffusivity (κ_j) of the soil and vegetation layers separately. This separation was necessary because temperature measurements were conducted with distinct instruments in each layer, and the measurements at the interface did not align perfectly. The offset is expected to be constant for the entire height of the measurement setup. This could be the effect of a slight discrepancy in the calibration of the setup. It does not affect the credibility of the observations, which can still be evaluated albeit in separate models.

It is important to note that the *thermal conductivity* of the layers cannot be analysed in this manner. Thermal diffusivity, κ is a parameter in the decoupled model (Eq. 3.2), while thermal conductivity, λ, exists only explicitly as a parameter in the coupled model (Eq. 3.4, 3.5).

Each section includes a detailed analysis of the observations and a discussion of their consistency with theoretical expectations.

4.1. Validation of the Two-Layer Model with the Analytical Solution

The numerical temperature profiles are compared to the analytic solution at different times to validate the two-layer model. The conditions for the model were matched with the conditions for the analytic solution, as specified earlier in Section 3.4. The analytical solutions were derived in Section 2.3.

Figure 4.1 illustrates the numerical temperature profiles at different times during the diurnal cycle. The numerical profiles were computed using the model and are represented by the coloured lines. The analytical solutions follow from Equations 2.13 and 2.12 are represented by dotted lines.

In Figure 4.1, it can be seen that the numerical profiles align closely with the analytical solution at all time steps. Near the interface, the correspondence between the analytical and numerical profiles is also strong. Minor discrepancies are present due to the discretisation. However, these differences are smaller than typical measurement errors and are therefore negligible for the implementation of the numerical model. The overall agreement with the analytical solution shows that the two-layer numerical model accurately describes diffusive heat transfer in two media.

4.2. Analysis of Soil Observations

Observed soil temperature profiles are analysed and compared to the decoupled model with different thermal diffusivities κ_{soil}. The varying nature of κ_{soil} makes it interesting to investigate the optimal value that minimises the difference between the model and data daily. The discrepancies for different thermal diffusivities are calculated to analyse the model's capability of replicating observed temperature

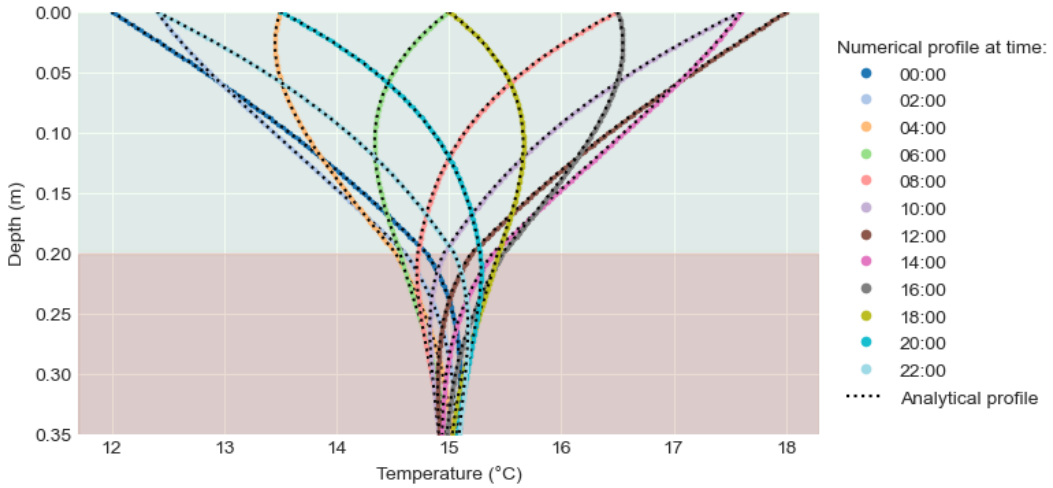

Figure 4.1: Representation of the numerical profile at different times, compared to the analytical solution following from Equations 2.13 and 2.12

profiles.

4.2.1. KNMI Soil Data

In this research, measurements from the Royal Dutch Meteorological Institute (KNMI) are used. Soil measurements are conducted in the Energy Balance (EB) field at Cabauw, 300 m North of the main tower. Pt100 elements are used as a measurement instrument. The measurement elements are buried at different depths of 0.4, 2, 4, 6, 8, 12, 20, 30, and 50 cm. The measurements have a 10-minute time resolution and are validated by the KNMI [17].

Figure 4.2 shows the observed temperature at all depths from June 1st till June 17th 2024. The uncertainty in temperature of the measurements is 0.008 ° C. In height, the uncertainty is 0.5 cm, meaning the sensor could be placed within a range of 0.5 cm above or below the given height.

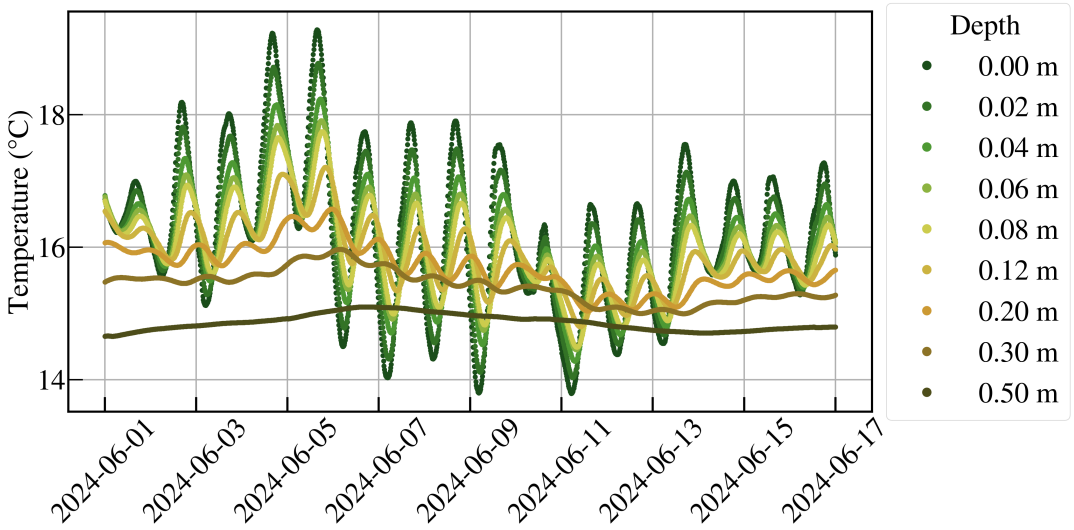

Figure 4.2: Soil temperature observations in June 2024 at Cabauw, the Netherlands. Temperatures are measured by the KNMI using probes at different heights inside the soil. [17]

From the data, a single day was selected arbitrarily for further research: June 7th. The observed temperatures on this day are presented in Figure 4.3.

In the figure, an amplitude decay can be observed, as the temperatures fluctuate more closer to the

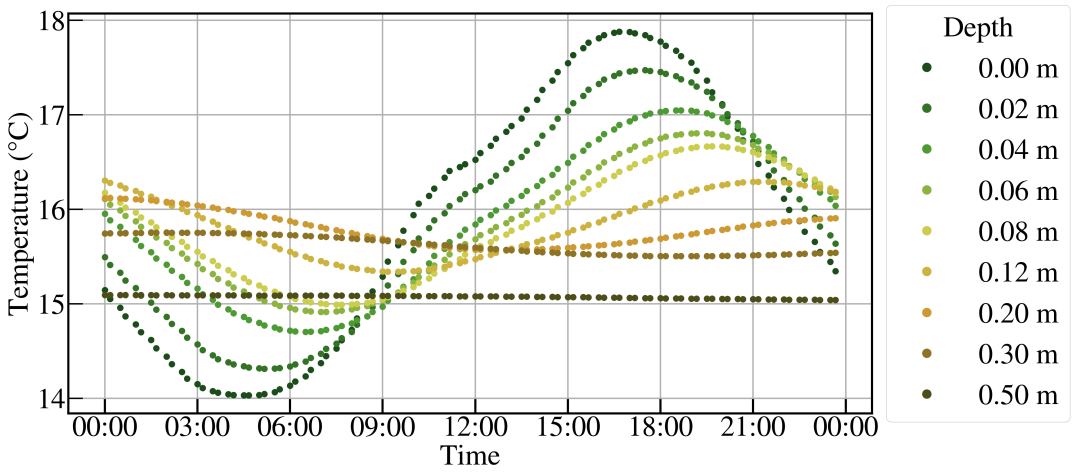

Figure 4.3: Validated soil temperature data for June 7th 2024 at different depths, with a 10-minute time resolution.

surface. A closer look also shows a phase shift of deeper layers compared to the shallow profiles. More irregular fluctuations are observed at the shallowest profiles of 0.00 m and 0.02 m. These represent high-frequency fluctuations, which are dampened deeper in the soil. This is in line with the expectations from the theoretical framework presented in Section 2.2 (frequency-dependent exponential decay). These higher frequencies are a consequence of, e.g., changing cloud cover.

4.2.2. Determining Thermal Diffusivity (κ_{soil})

The model was executed for different κ_{soil} values and the root mean squared error (RMSE) was calculated between simulated and observed soil temperature profiles using Equation 3.10. The calculated RMSE at the optimum is 0.053° C, obtained for $\kappa_{soil} = 3.2 \cdot 10^{-7}$ m^2 s^{-1}.

For this optimal diffusivity, the temperature profiles are reconstructed. Figure 4.4 shows the measured data in points against the model data existing at multiple heights N_z.

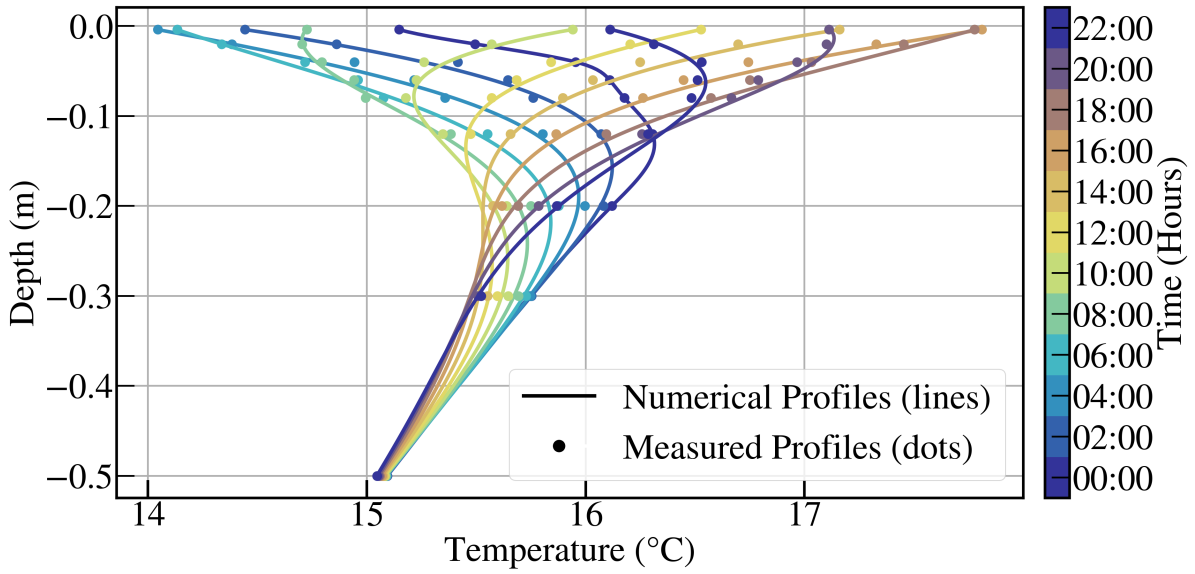

Figure 4.4: Vertical soil temperature profiles at different times. The observed temperatures are indicated with dots and the temperature profiles following from the model are represented by lines. The numerical profiles are calculated with the optimal value: $\kappa_{soil} = 3.2 \cdot 10^{-7}$m^2 s^{-1}. The RMSE for this κ is 0.053 ° C

The temperature profile is shown at different times. The top and bottom points, as well as the initial profile at 00:00 h, are imposed as boundary and initial conditions to the model. There should be per-

fect correspondence in these points. A bigger discrepancy is seen in the highest layers, where the observations fluctuate more. The discrepancy is fairly small at deeper heights, 0.2 m and 0.3 m. A reason for these discrepancies can lie in the measurement error of the KNMI data. The error in the temperature measurements from the used instruments has a very low value of $0.008C$ [17], however, the depth of the measurement setup can vary up to 5mm higher or lower [9]. This has bigger effects on the model in the measurement-dense area (top of the soil) than in the area where measurements are sparse (deeper inside the soil), due to the high gradient in the temperature profile near the surface.

It is known that κ_{soil} may slowly vary over time, as a result of, e.g., changing soil moisture content. Therefore, the optimal value is calculated for each day in the measurement set of June 2024. Figure 4.5 shows the relationship between the RMSE and κ for all days in the dataset.

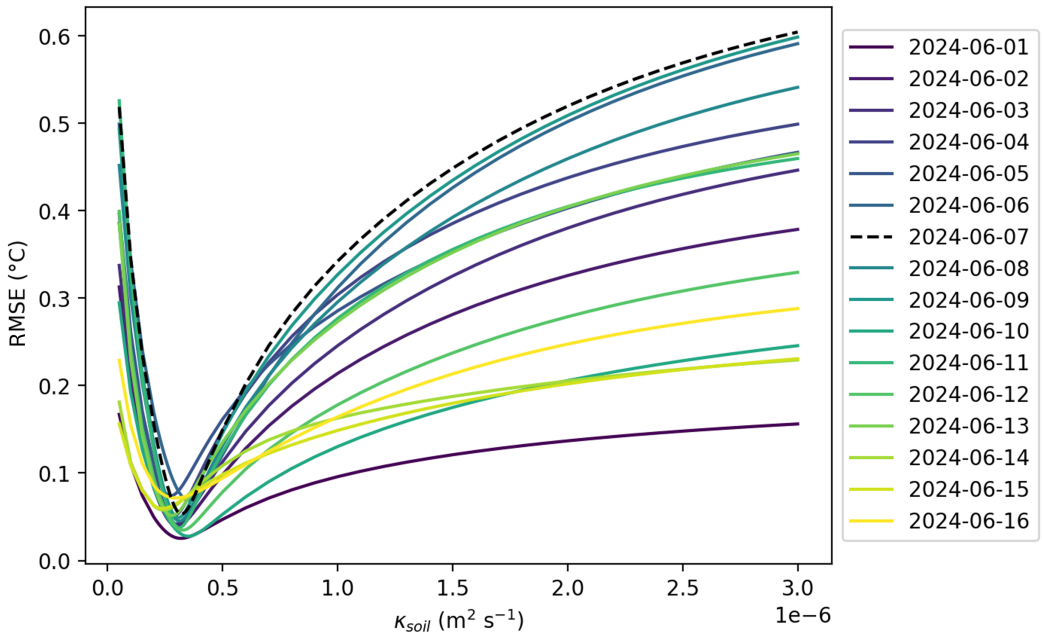

Figure 4.5: RMSE curve for different κ_{soil}'s for all days in the dataset.

The mean of all the optimal $\kappa's$ in this dataset is $3.0 \pm 0.3 \cdot 10^{-7}$m^2 s^{-1}, which is in line with previous research [9, 18, 19, 20]. Outside the optimum, the discrepancies between the model and the measurements increase. This stresses the importance of accurately estimating the thermal diffusivities for reliable model predictions.

Overall, the results show that the decoupled one-layer model accurately reproduces the observed soil temperature dynamics and can find the daily optimal thermal diffusivity values. While for lower depths minor discrepancies were observed, these are within acceptable bounds given possible errors in measurement data. This analysis proves the model's applicability to the soil layer.

4.3. Analysis of Grass Observations

This section focuses on analysing the observed temperature dynamics within the grass layer to evaluate the applicability of the decoupled one-layer model for vegetation. Similar to the soil analysis, the goal was to identify the optimal thermal diffusivity (κ_{veg}) for the grass layer by comparing observed temperature profiles with model simulations. Observations were conducted at Cabauw in June 2024, providing high-resolution data on diurnal temperature variations within the grass canopy. The analysis includes an examination of the temperature profiles, a comparison of model simulations with observations, and an evaluation of the phase shift behaviour within the grass layer. These steps aim to evaluate the extent to which the model captures the thermal dynamics of the vegetation layer.

4.3.1. Grass Coil Data

The temperature data for the grass layer was collected using a DTS-based (distributed temperature sensing) coil measurement setup [10]. This measurement technique uses fibre optic cable to probe temperatures with a 25 cm resolution. The coil is 1 meter high with a vertical resolution of 1.25 mm and an accuracy of 0.1 ° C. The high vertical resolution provides information needed for in-depth analysis of temperature profiles inside the grass canopy. More details about the design and calibration of the coil can be found in Ter Horst et al. (2024) [10].

The coil was positioned at Cabauw, near the EB field where the soil measurements were executed. The used dataset from the field experiment runs from the 1st of June till the 17th of June 2024. Measurements have a 5-second time resolution and are time-averaged to a 10-minute resolution. Figure 4.6 shows the observed temperature in the selected period. A selection in height was made to display only every 16^{th} other point. However, all measured heights are used in the numerical model.

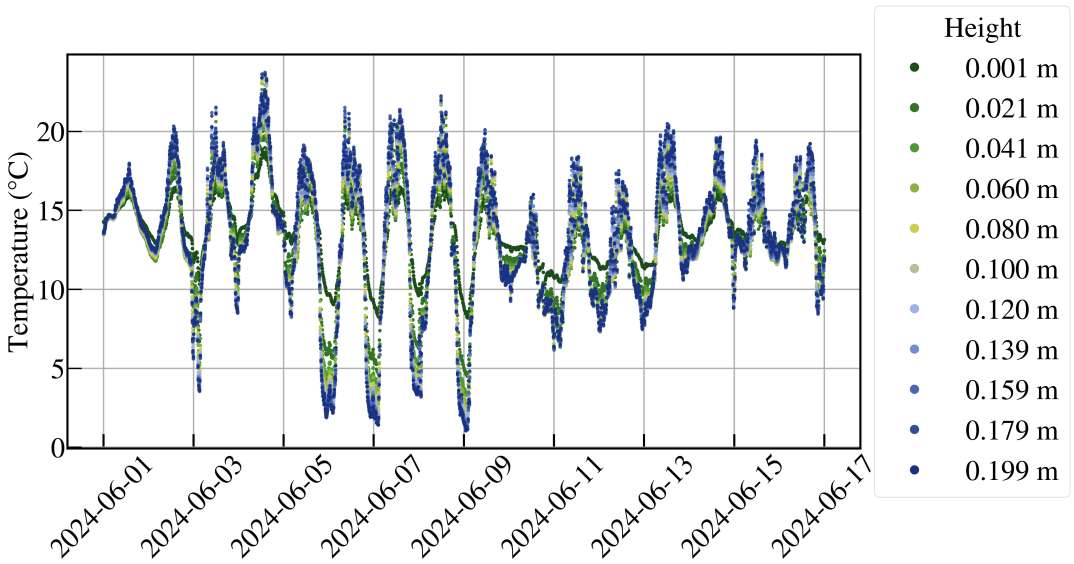

Figure 4.6: Grass temperature observations at selected heights in June 2024 at Cabauw, the Netherlands. Measurements were conducted with a DTS coil and were averaged over 10 minutes [10].

For detailed analysis, a single day was selected from the dataset. In line with the soil analysis, June 7th was selected. Figure 4.7 illustrates the observed temperature profile for this day. One of the typical characteristics of the diffusive model is visible in Figure 4.7; amplitude decay. Closer to the ground, the temperatures are higher during nighttime while during daytime the temperatures are lower compared to measurements higher up in the grass. The second characteristic, phase shift, is barely recognised in this figure. High-frequency signals caused by cloud cover fluctuations have an effect at all heights within the grass layer.

4.3.2. Model-Data Comparison

To determine the optimal values for the thermal diffusivity for the grass layer, the observed temperature profiles are compared with model simulations. Figure 4.8 shows the data for the selected day, June

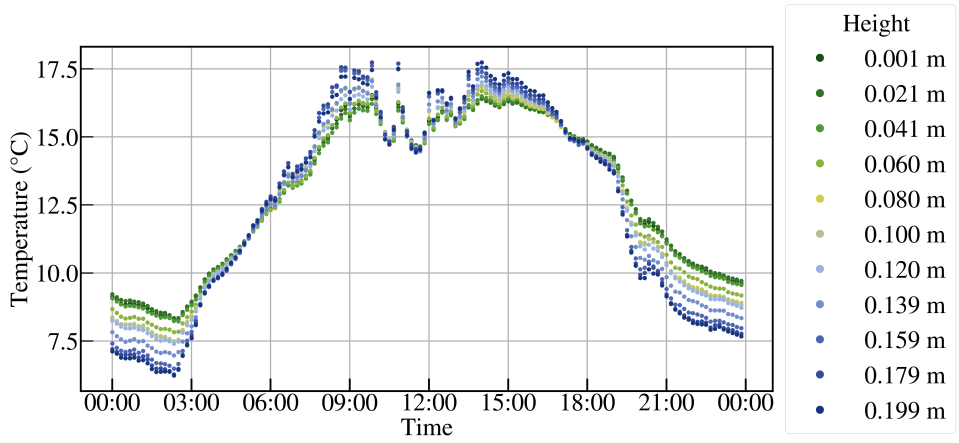

Figure 4.7: Grass temperature data for June 7th 2024 at selected depths, 10 minute averaged. A diurnal signal is recognised from the incoming solar radiation, with high-frequency signals during daytime caused by cloud cover fluctuations.

7^{th}, at different times. For comparison, the figure also shows the numerically calculated profiles with the expected κ_{veg} value found by Linden et al. [9].

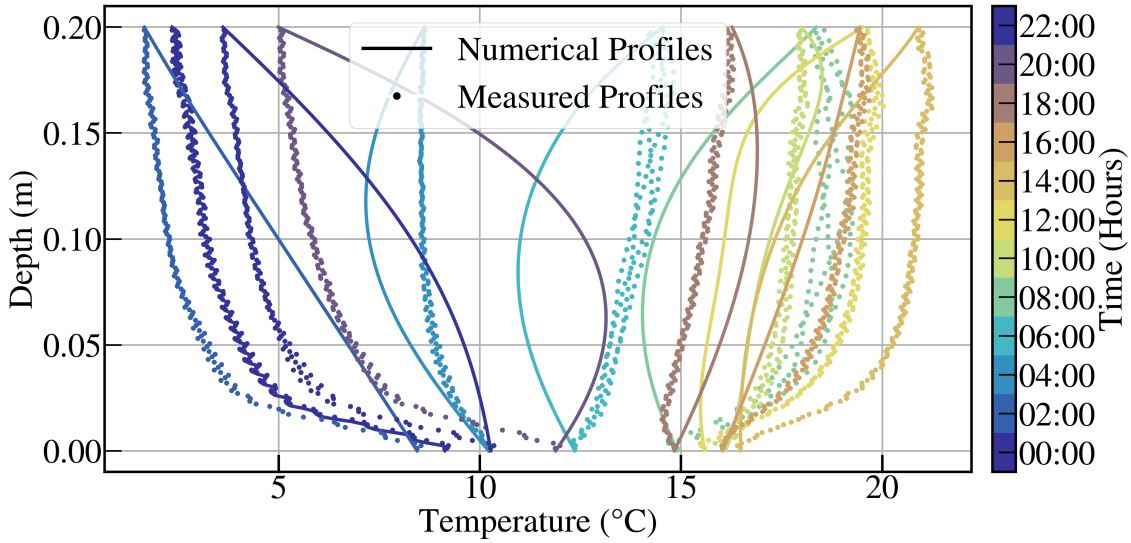

Figure 4.8: Vertical temperature profiles measured inside the vegetation at different times, compared to temperatures following from the numerical model with $\kappa_{veg} = 12 \cdot 10^{-7} \text{m}^2\ \text{s}^{-1}$

Figure 4.8 indicates that the model has a qualitatively different shape from the field measurements. Because the profiles do not correspond on a qualitative level, the measurements cannot be used to find an optimal value for κ_{veg} . This leads to the conclusion that the diffusive model is not able to replicate the temperature profiles inside the grass layer.

4.3.3. Phase Shift Analysis

Additionally, an analysis of phase shifts within the grass layer is performed to determine whether the phase shifts of the temperature profiles follow purely diffusive (linear) behaviour or deviate due to additional mechanisms. As outlined in Section 4.3.2, Figure 4.7 did not reveal a discernible phase shift within the grass layer. The absence of a noticeable phase shift suggests that the purely diffusive model may not accurately represent the observed dynamics in this region. To investigate this further, a single frequency was isolated, and the associated phase shift was analysed.

The diurnal frequency component is the most prominent frequency in the data making it the most suitable choice for the phase shift analysis. Figure 4.9 presents the measurements of June 7th, filtered in

the Fourier spectrum to isolate the diurnal frequency along with the mean (DC-component). The black dots in the figure indicate the peaks of the periodical signal, and their temporal positions are analysed to examine the phase shift within the grass layer.

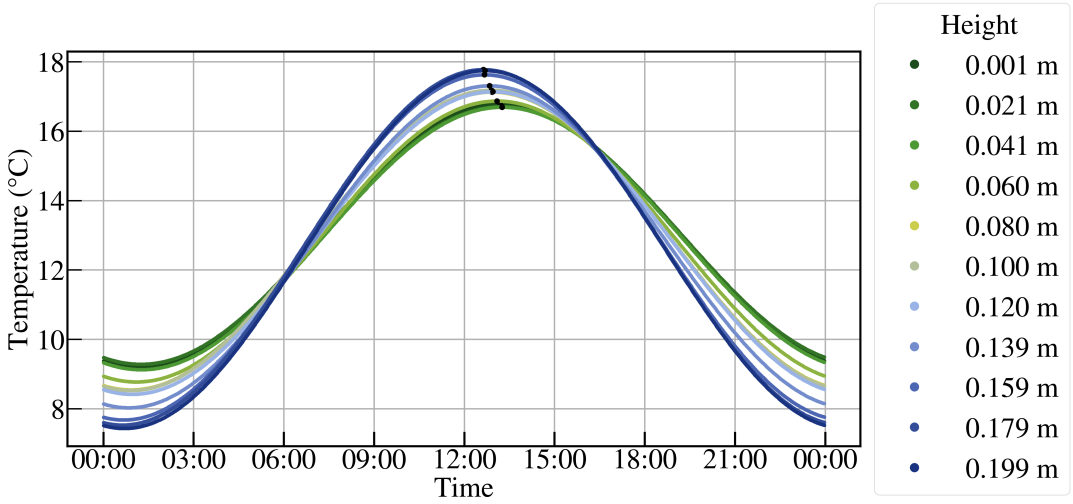

Figure 4.9: Filtered diurnal component of the grass temperature data for June 7th 2024. Black dots are put at the location of the tops of the sines and are used for phase shift analysis.

Figure 4.9 indicates a phase shift of approximately one hour across the total height of the grass layer. Additionally, the black dots suggest a linear phase shift with height. However, the limited number of displayed heights and the lack of zoomed detail in the figure may conceal the full extent of the phase shift. To provide a more detailed analysis, in Figure 4.10 the temporal locations of the maxima of the periodic signal at all measured heights are compared to the temporal location of the maximum of the signal at the top of the grass layer. This comparison is presented as the phase shift, ϕ, with respect to the highest point in the vegetation.

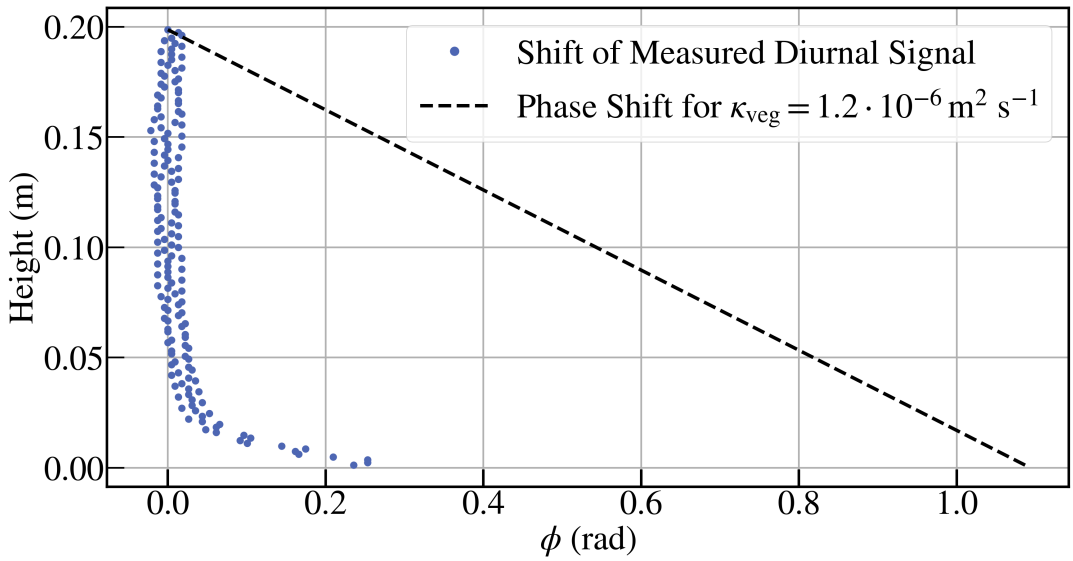

Figure 4.10: Comparison between the observed phase shift in grass for the diurnal frequency (blue dots) and the expected linear phase shift for the diurnal frequency with $\kappa_{veg} = 12 \cdot 10^{-7}\text{m}^2\ \text{s}^{-1}$

Figure 4.10 illustrates that the phase shift of the diurnal frequency in the upper portion of the vegetation is negligible. However, within the lowest 2.5 cm, a linear phase shift with height is observed. This suggests that additional physical processes, such as convection and radiation, are influencing the

system in the upper section of the vegetation. Therefore, the purely diffusive model fails to adequately describe the dynamics of the grass layer.

These limitations of the purely diffusive model suggest the need for an alternative approach that accounts for the influence of other physical processes within the grass layer. The next chapter introduces a revised model, incorporating a source term, to better replicate the measured temperature profiles within the grass layer.

5

Provisional Source Term Correction

In the previous chapter, it was shown that a purely diffusive model fails to adequately describe the dynamics within the grass layer. The observed temperature profiles exhibit qualitatively different behaviour from the diffusive model. This mismatch cannot be attributed to an incorrect estimate of the thermal diffusivity, κ_{veg}. Instead, this suggests that essential physical processes have been incorrectly neglected.

The aim of the numerical model is to accurately replicate the temperature dynamics within the grass layer while maintaining low complexity and minimising the number of parameters. If the model proves to be too simplified to describe the temperature dynamics, additional complexity must be introduced.

Several assumptions were initially made to delineate the purely diffusive model. Now, given the observed *qualitative* discrepancy, additional complexity must be introduced to better capture the underlying physics. Processes such as radiation, evapotranspiration (dew formation), and wind penetration (convection) likely play a larger role than initially assumed. However, incorporating a fully detailed representation of these processes would increase model complexity significantly, compromising its simplicity.

Figure 4.8 suggests that an additional energy source may be missing. Radiative heating/cooling is an important process that likely contributes to the observed missing energy. In this research, radiative heat transfer is selected as the next step to improve model accuracy, with cooling at night and warming during the day.

This chapter presents a provisional radiative source term correction to the model, acknowledging that other processes, such as evapotranspiration, may also influence the system but are currently beyond the scope of this study. By introducing this additional physical mechanism, the model aims to better reproduce the observed temperature profiles within the grass layer.

The chapter begins with a non-dimensional analysis to evaluate the effect of adding a source term. The non-dimensional solution is then derived and plotted for different values of the source term. Finally, a numerical implementation of the source term is conducted. The results are compared to the purely diffusive model to evaluate improvements in capturing the observed temperature variations.

5.1. Non-Dimensional Analysis

Before implementing a more exact numerical implementation, a non-dimensional analysis is performed. The non-dimensional analysis is typically used to evaluate the relative importance of different physical processes on the solution, in this case, the (non-dimensional) temperature profile [21]. The primary goal of the non-dimensional analysis is to reduce the number of parameters governing the problem. The parameters that govern the diffusive transport are weighed against the radiative source term, resulting in a single dimensionless variable, γ, governing the temperature variations.

The source term introduced in this study represents radiative heating and cooling within the grass layer.

Radiation undergoes extinction inside the canopy, which is commonly modelled using the Lambert-Beer law, that is an exponential decay with depth. This approach is used in atmospheric models such as ECMWF [22] and the CLASS model [23]. However, for simplicity, this research initially adopts a linear decay to assess the general effect of an added source term. The optimal formulation of the source term can be explored in future research. Consequently, the radiative source term is formulated as:

$$S(z) = S_0 \left(1 - \frac{z}{\delta}\right), \tag{5.1}$$

where S_0 [W m^{-3}] is the value of the source at the top of the canopy and δ [m] is the canopy height.

When this linear source term is incorporated into the purely diffusive heat equation (Eq. 2.4), the governing equation for the temperature within the vegetation layer becomes:

$$\frac{\partial T_{veg}}{\partial t} = \kappa_{veg} \frac{\partial^2 T_{veg}}{\partial z^2} + \frac{S(z)}{\rho_{veg} c_{veg}}, \tag{5.2}$$

where T_{veg} is temperature [° C], κ_{veg} is the thermal diffusivity [m^2 s^{-1}], S is the depth-dependent source term [W m^{-3}], ρ_{veg} is the density [kg m^{-3}] and c_{veg} is the specific heat capacity [J kg^{-1} °C^{-1}].

The temperature profile within the grass layer maintains its overall shape but shifts uniformly over time around midday and midnight, see Figure 4.8. This behaviour is evident in the figure, where the profiles at $00:00$ and $02:00$, as well as those at $12:00$ and $14:00$, have nearly identical shapes with a uniform temperature shift. In contrast, the profile shape changes significantly at intermediate times (e.g., $16:00$ and $18:00$). Therefore, the behaviour of the midday and midnight profiles is used to estimate the absolute value of the source term, P.

Based on this behaviour, the vertical temperature gradient is approximated as steady, leading to the assumption:

$$\frac{\partial}{\partial t}\left(\frac{\partial T_{veg}}{\partial z}\right) = 0, \tag{5.3}$$

which can be rewritten as:

$$\frac{\partial}{\partial z}\left(\frac{\partial T_{veg}}{\partial t}\right) = 0. \tag{5.4}$$

Integrating both sides over z gives:

$$\frac{\partial T_{veg}}{\partial t} = C, \tag{5.5}$$

where C is an integration constant representing the constant cooling or warming over height.

In the following analysis, we subtract the overall system cooling/warming rate, C, treating it as negligible. While the assumption $C \approx 0$ is **not** strictly valid for the situation shown in Figure 4.8, it holds on certain days (see, Appendix A). For this preliminary analysis, the goal is to obtain an initial estimate of the source term, making this approximation acceptable.

Applying the quasi-steady state assumption, Equation 5.2 simplifies to:

$$0 = \kappa_{veg} \frac{d^2 T_{veg}}{dz^2} + \frac{S(z)}{\rho_{veg} c_{veg}}. \tag{5.6}$$

Physically this occurs when both the conductive heat transport and the radiative heating have much shorter timescales than the diurnal temperature variations at the surface.

Dimensionless temperature and depth are introduced as follows:

$$\hat{T} = \frac{T_{veg} - T_\delta}{T_0 - T_\delta}, \qquad \hat{z} = z/\delta, \tag{5.7}$$

where T_0 is the temperature at the top of the canopy ($z = 0$) and T_δ is the temperature at the surface ($z = \delta$). The definitions of $\hat{T}$ and $\hat{z}$ normalize the temperature and depth between the top and bottom of the canopy.

With the introduction of the dimensionless temperature $\hat{T}$ and depth $\hat{z}$, the effect of a radiative source term on the temperature profile can be conceptualized. To illustrate this effect, standard temperature profiles for daytime and nighttime conditions are considered. Figure 5.1 shows diffusive temperature profiles, transformed by the inclusion of a radiative warming source during the day and a radiative cooling source during the night.

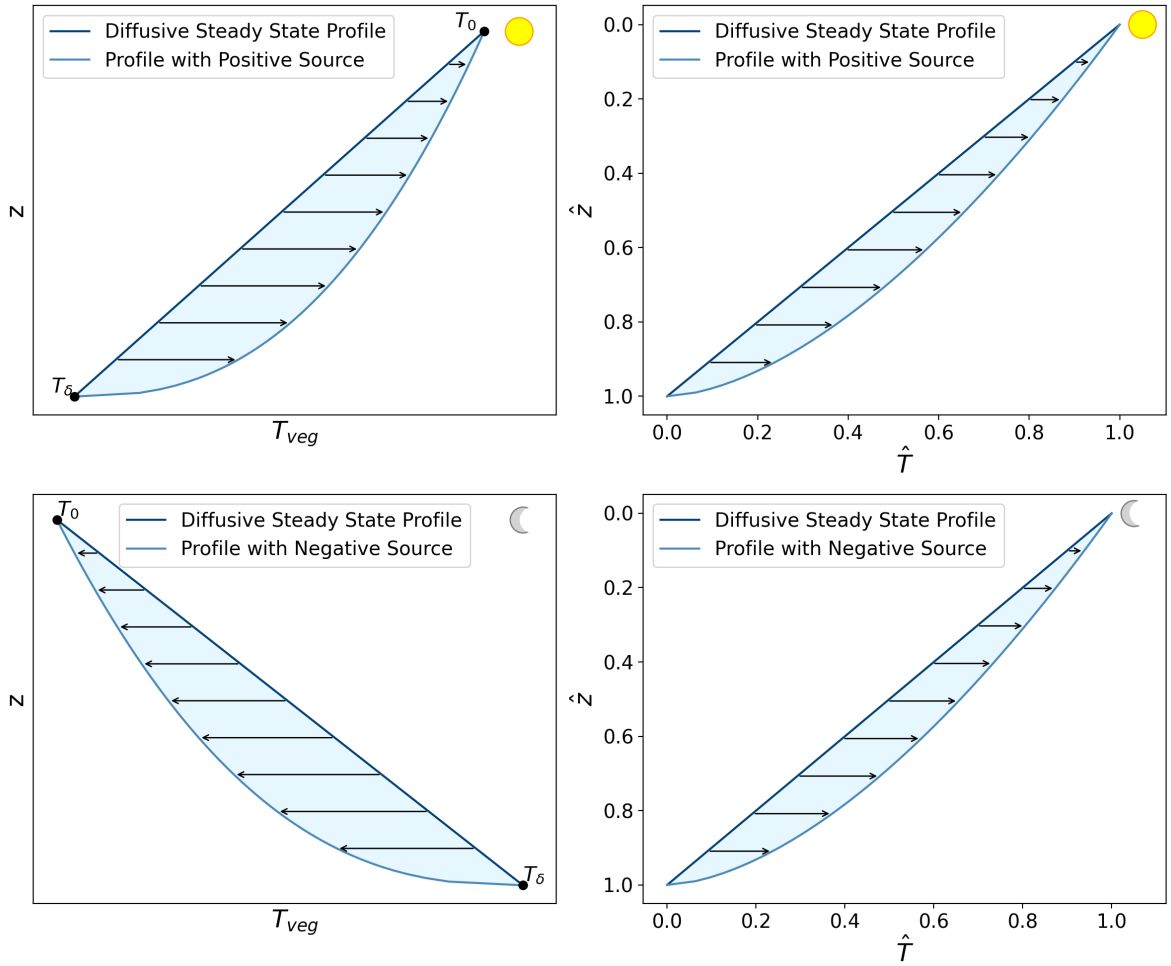

Figure 5.1: Conceptual graphs of temperature profiles for daytime (top) and nighttime (bottom) conditions. Each plot shows a steady state diffusive profile, both with and without local radiative sourcing according to Eq. 5.1, with warming during the day, and cooling during the night. The arrow represents decreasing γ (or increasing source). During the day, the top of the grass has a higher temperature (T_0) compared to the ground surface (T_δ). For nighttime, this is the other way around. On the right-hand side, the situation is depicted as the dimensionless temperature $\hat{T}$ and depth $\hat{z}$ from Equation 5.7.

The conceptual profiles illustrate the expected shape of the profiles transformed by the source. The right-hand side profiles show how the dimensionless temperature profiles are impacted by this transformation. When the non-dimensional analysis is completed, these profiles provide a reference to assess the right value of the dimensionless variable.

Moving on with the non-dimensional analysis, the dimensionless temperature and depth are substituted into Equation 5.6. This results in:

$$0 = \frac{\kappa_{veg}\,(T_0 - T_\delta)}{\delta^2}\frac{d^2\hat{T}}{d\hat{z}^2} + \frac{S_0}{\rho_{veg}c_{veg}}\,(1-\hat{z})\,. \tag{5.8}$$

Rearranging this gives the following equation:

$$0 = \gamma\frac{d^2\hat{T}}{d\hat{z}^2} + (1-\hat{z})\,, \tag{5.9}$$

where the dimensionless parameter γ, that describes the relative importance of conductive heat transfer and the source term. It is defined as:

$$\gamma = \frac{\kappa_{veg}\rho_{veg}c_{veg}\left(T_0 - T_\delta\right)}{S_0\delta^2}. \tag{5.10}$$

In this expression, two terms can be negative: $(T_0 - T_\delta)$ and S_0. During daytime, $(T_0 - T_\delta)$ is positive. Since radiative warming adds energy, S_0 is also be positive. Conversely, during nighttime, $(T_0 - T_\delta)$ is negative. In this case, S_0 is also negative, as radiative cooling corresponds to a loss of energy. When $\gamma \gg 1$, the diffusive term dominates and the temperature profile approaches a linear form. For the expected behaviour with a significant contribution of the source term, γ is expected to be positive and less than 1, both during day and night.

Integrating Equation 5.9 twice over $\hat{z}$ transforms it to:

$$\hat{T} = -\frac{1}{\gamma}\left(\frac{\hat{z}^2}{2} - \frac{\hat{z}^3}{6}\right) + C_1\hat{z} + C_2, \tag{5.11}$$

where C_1 and C_2 are integrating constants. To solve this equation for C_1 and C_2, the boundary conditions (BC's) for temperature must be rewritten in their dimensionless form. The dimensionless boundary conditions are obtained by filling in the top and bottom temperatures into Equation 5.7. At the top of the grass, the temperature is $T_{veg} = T_0$ and $z = 0$, for both daytime and nighttime. This gives the dimensionless top BC:

$$\hat{T}\left(0\right) = \frac{T_0 - T_\delta}{T_0 - T_\delta} = 1, \qquad \hat{z} = \frac{0}{\delta} = 0. \tag{5.12}$$

At the ground surface, the temperature is $T_{veg} = T_\delta$ and $z = \delta$. The dimensionless BC at the surface then becomes:

$$\hat{T}\left(1\right) = \frac{T_\delta - T_\delta}{T_0 - T_\delta} = 0, \qquad \hat{z} = \frac{\delta}{\delta} = 1. \tag{5.13}$$

Solving Equation 5.11 for C_1 and C_2 using these dimensionless boundary conditions leads to the general solution:

$$\hat{T} = -\frac{1}{\gamma}\left(\frac{\hat{z}^2}{2} - \frac{\hat{z}^3}{6}\right) + \left(\frac{1}{3\gamma} - 1\right)\hat{z} + 1. \tag{5.14}$$

In Figure 5.2, this solution is illustrated. The value of γ is varied to observe its effect on the shape of the temperature profile.

Figure 5.2 shows that the dimensionless temperature profile bends in the expected direction for positive values of γ. The profile for $\gamma = 0.3$ is close to the profile in the conceptual plot (Fig 5.1). However, the curvature at the top appears to be too pronounced, while the bending at the bottom is less than expected. This suggests that the assumption of a linear source term may require adjustments to better reproduce the temperature profile behaviour.

The non-dimensional analysis confirms that the introduction of a radiative source term leads to temperature profiles that better reflect the observed behaviour. The ideal form of the source term requires further investigation to improve the model even more.

5.2. Linear Source Term in the Numerical Model

The non-dimensional analysis showed that incorporating a source term improved the temperature profiles compared to the purely diffusive model.

Building on these findings, a numerical implementation is performed. The source term is incorporated into the two-layer diffusive model with a diurnally varying temperature at the top. Since the diffusive model performed sufficiently for the soil, the source term is only applied within the vegetation layer, leaving the soil purely diffusive.

The implemented source term follows the linear formulation described in Equation 5.2. However, as observed earlier, S_0 must vary over time, having a negative value during the night for radiative cooling,

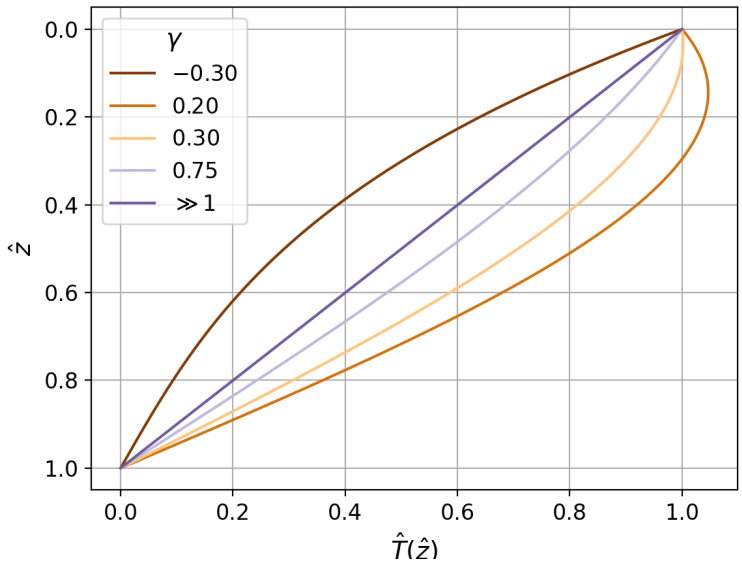

Figure 5.2: Non-dimensional temperature profiles for a quasi-steady state situation with a linear source term. The magnitude of the source term is varied, shown here as a varying γ value.

and a positive value during the day for radiative warming. This time dependency is incorporated by describing the source term as:

$$S(z,t) = S_0(t)\left(1 - \frac{z}{\delta}\right) = P \cdot \cos(\omega_{day} t + \pi)\left(1 - \frac{z}{\delta}\right), \tag{5.15}$$

where P [W m^{-3}] is the absolute magnitude of the source term, ω_{day} [s^{-1}] is the diurnal frequency and a phase-shift of π ensures the source term is negative during the night and positive during the day, with $t = 0$ corresponding to midnight.

The value for P is calculated from Eq. 5.10, with $S_0 = P$ and $\gamma = 0.3$. This source is then added to Eq. 3.2, to implement the source term in the numerical model.

Figure 5.3 illustrates the resulting temperature profiles from the numerical implementation with and without source term. In this way, the impact of incorporating such a term on the time-dependent shapes of the temperature profiles can be evaluated.

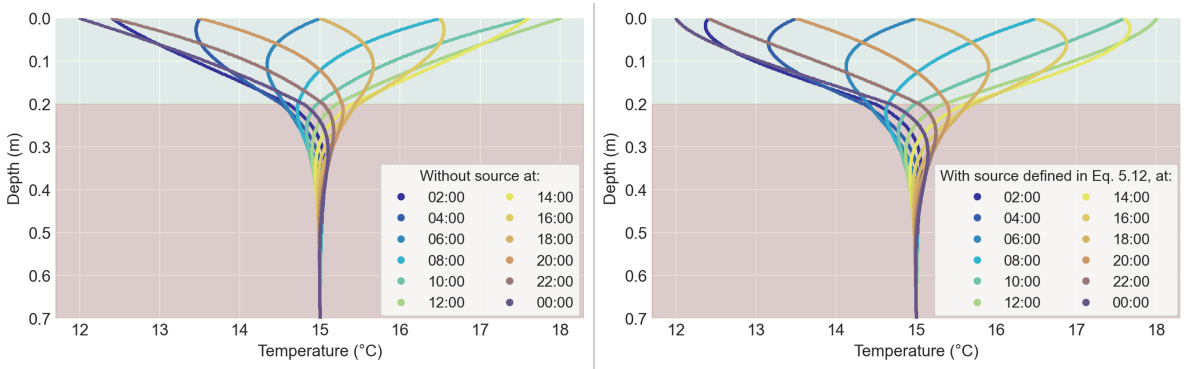

Figure 5.3: Temperature profiles within the purely diffusive two-layer model (left) and the two-layer model with radiative source term within the vegetation layer (right) at different times during the diurnal cycle.

The illustration on the right presents the two-layer model with a radiative source term. Compared to the purely diffusive model (left) the modified model produces temperature profiles that more closely

resemble the observed temperature profiles. In the observed profiles, the gradient at the top of the grass layer is minimal (see Fig. 4.8). In contrast, for the profiles of the adjusted model, a temperature gradient ($\frac{dT}{dz}$) is present, suggesting further refinement is needed. Additionally, the steep temperature gradient observed near the surface is less pronounced and starts higher in the model with source, indicating that the linear dependency of the source term may not fully capture physical reality.

Introducing a radiative source term into the numerical model improves its ability to reproduce observed temperature profiles within the grass layer. While the adjusted model captures key trends more effectively than the purely diffusive approach, discrepancies remain, particularly in the vertical temperature gradient near the surface. These findings suggest that further modifications, such as refining the source term's functional form or incorporating additional physical processes, may be necessary to achieve a more accurate representation of temperature dynamics.

6

Discussion and Recommendations

The results confirm that diffusive modelling accurately describes soil heat transport but fails to capture temperature dynamics within the vegetation layer. Specifically, the purely diffusive model tends to underestimate daytime temperatures and overestimate nighttime temperatures, suggesting additional warming during the day and cooling at night. To ensure the reliability of the data used for model validation, this chapter further examines potential biases and artefacts. The observed discontinuity between soil and vegetation temperature data is analysed in detail, demonstrating that it likely represents a constant bias and that the shape of the profiles themselves is not affected.

To investigate why the diffusive approach proposed by Linden et al. [9] does not adequately describe the vegetation layer, key initial model assumptions are revisited, proposing suggestions for future studies. Additionally, the formulation of the provisional linear source term is discussed in greater detail.

6.1. Data Reliability and Temperature Discontinuity at the Interface

For the analysis of the model, temperature observations from the KNMI within the soil and DTS coil measurements within the vegetation layer were used. In previous studies by the KNMI, the KNMI validated the observations within the soil layer [17]. The coil temperature profiles were cross-validated against KNMI measurements at 10 cm and 1,5 metres [17, 10], confirming the reliability of both datasets.

Despite the validation, awareness of potential measurement artefacts and biases is necessary to ensure accurate interpretation of the data. As a result of environmental influences, such as radiative effects and precipitation, measurement uncertainties are introduced in the coil temperature measurements. In a majority of cases, this results in an offset of the measured temperature profile with regard to the KNMI measurements. This offset is assumed to be constant over height, not affecting the relative temperature gradients within the grass layer. This means that the shape of the profile is conserved in most cases, allowing analysis of the temperature profile. In further research, radiative corrections can be applied to improve accuracy.

Additionally, the soil temperature observations may be affected by discrepancies in the sensor height, that is $T(z,t)$ may be affected by uncertainties in the exact observational depths. These uncertainties are not explicitly mentioned in the KNMI report[17]. It is known that the soil temperature sensors experience a slight decrease in height over time, due to soil settling [private communication Reinder Ronda (KNMI)]. A deviation in sensor height is particularly significant near the surface, where temperature gradients are steep, which implies that a small error in observational depth leads to a significant error in temperature.

Although both datasets are validated, a temperature discontinuity remains at the vegetation-soil interface, making it impossible to evaluate heat transfer across the surface in a coupled model. To address this, two decoupled models were employed to analyse each layer independently. Figure 6.1 illustrates the temperature observations by the KNMI, taken just below the surface ($z = -0.004$ m), compared to the coil observations, taken just above the surface ($z = 0.001$ m).

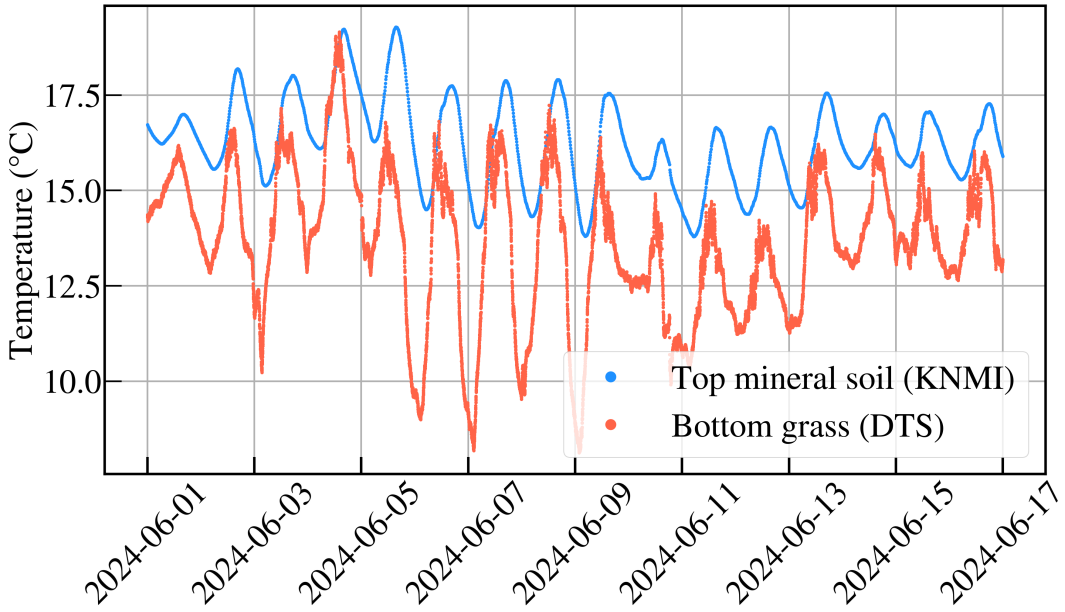

Figure 6.1: Comparison of the KNMI validated observations within the mineral soil, just below the surface ($z = -0.004$ m) [17], with DTS coil observations, taken just above the surface ($z = 0.001$ m) [10].

The figure shows that the temperature observations are not likely to be continuous across the surface. The previously mentioned measurement uncertainties are not significant enough to explain the bias in Figure 6.1. A possible other factor contributing to this discontinuity is the measurement environment. The vegetation layer measurements were obtained from a fibre optic cable surrounded by air, whereas the soil sensors were embedded in the mineral soil. Differences in heat transfer to the temperature sensors within these environments can influence recorded temperature, causing the observed discontinuity. Another potential explanation for the discrepancy is the sensor placement. The sensors were located in neighbouring fields at the same location. Their horizontal separation is approximately 10 metres. Small variations in surface elevation (on a centimetre scale) between the measurement locations could introduce offsets in the data.

For future research, it is recommended to refine the Cabauw experiment by executing all measurements at the same location. Ideally, the measurements should be obtained using the same sensor in the soil and vegetation layers. A potential approach is to partially bury the DTS coil into the ground, in combination with an extended soil temperature measurement. An extension of the DTS measurements into the ground, in the form of a screw, was recently investigated by Schilperoort et al. [24]. However, when burying the coil or screw, a settling period is required to allow the soil to stabilize and the grass to regrow before the measurements can be considered representative. Since the top section of the soil screw remains above ground, it is not subject to overgrowth by grass.

Moreover, the scope of the field experiment could be extended beyond temperature measurements, to include in-grass wind, dew formation, and radiation measurements, to create extra observational redundancy. These additional observations could help to fully quantify the in-grass microclimate and would help to quantify other heat transfer processes at play.

6.2. Source Term Formulation

As demonstrated in Chapter 5, the incorporation of a linear source term improves the consistency with observed temperature profiles. However, discrepancies remain in the near-surface region. While this research discussed a provisional correction for radiative effects, it should be noted that other heat transfer processes, such as convection [25] and evapotranspiration [26] [18], may also influence heat transfer within the grass layer.

Temperature profiles from the data seem to follow a diffusive pattern in the near-surface part of the vegetation. In the results (Figure 4.10), this was observed as a linear phase shift in the lower few cm,

while the phase shift was less prominent higher in the canopy. Previous research on airflow over short, flexible vegetation supports this observation.

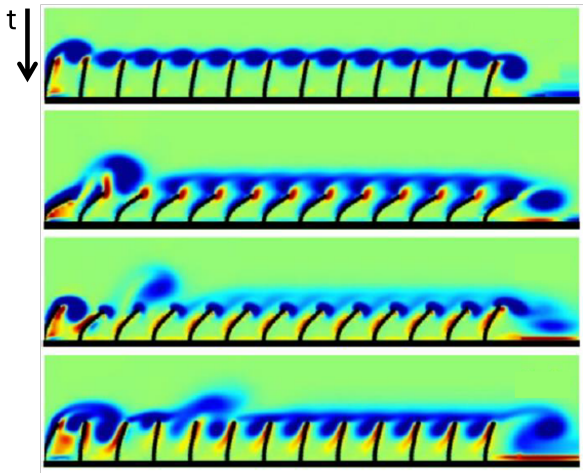

Figure 6.2: Airflow over flexible vegetation generates vortices within the grass layer. Blue represents negative vorticity. while red represents positive vorticity. Adapted from Sauerbier [25].

As shown in Figure 6.2 the airflow generates vortices within the grass layer, but their influence diminishes closer to the surface. This suggests that the near-surface vegetation is relatively shielded from wind effects. However, other heat transfer processes, such as dew formation and radiation, may still influence the near-surface region. Thus, incorporating an appropriate source term could further improve the accuracy of the modelled temperature profile in this area.

Additional research is needed to refine the source term. This can be done in two ways:

1. **A physically motivated approach** could extend the Lambert-Beer law to examine exponential radiative energy decay.
2. **A data-driven approach** could optimize the source term at each height based on measured temperature profiles or by using explicitly measured heat transfer processes.

For the latter, field experiments should be extended to include, e.g., radiation measurements, to quantify the heat transfer processes at play. The refined formulation of the source term would provide a more precise representation of heat transfer within the vegetation layer. If a generalisable formulation can be established, this could enable new, simplified representations of complex heat transfer within vegetation in land surface models.

6.3. Definition of the Grass-Atmosphere Interface

One of the initial model assumptions is the definition of the top of the grass layer. In this research, a fixed boundary is assumed, with the atmosphere above and the grass layer below. However, in reality the transition from vegetation to air is gradual. This may be causing the discrepancies between the observed and the modelled temperature dynamics.

Figure 6.3 shows the gradual transition from the atmosphere to the grass layer.

The figure illustrates the measurement setup where grass blades extend into the air at varying heights, which complicates defining *the* 'top' of the grass. Also, the height of the grass surrounding the DTS coil was not meticulously monitored for the duration of the field experiment. In this research, the grass height was measured at the beginning and end of the campaign. These heights were then averaged to obtain the used grass height: $\delta = 20$ cm, which is an approximation of reality.

It is recommended to explore alternative definitions of this 'top' interface. Additionally, it is recommended to monitor the grass height more closely when this field experiment is repeated.

Figure 6.3: The DTS coil at Cabauw with the grass field where the measurements were executed. Note that the grass is not uniform in height.

7

Conclusion

This research investigated the applicability of a diffusive approach to in-canopy heat transfer using a numerical model to describe temperature profiles within the vegetation-soil continuum.

The purely diffusive model accurately described temperature profiles within the soil layer, confirming that the thermal diffusivity (κ_{soil}) remains relatively constant over time. The optimal value found, $\kappa_{soil} = 3.0 \pm 0.3 \cdot 10^{-7}$ m^2 s^{-1}, is in line with previous research, reinforcing the model's accuracy for soil heat transfer.

However, the observed temperature profiles qualitatively disagree with the diffusive model in the vegetation layer. The diffusive model underestimates temperatures during the day and overestimates temperatures at night compared to the observations. The qualitative disparity between model and observational behaviour suggests that additional heat transfer processes, beyond pure diffusion, influence in-canopy temperature dynamics. Consequently, attempting to determine an 'optimal' thermal diffusivity for the vegetation layer is not meaningful, as additional heat transfer processes dominate temperature dynamics. A phase shift analysis further confirmed that the observed temperature profiles deviate from purely diffusive (linear) behaviour.

To address this limitation, a preliminary adjustment incorporating a linear source term improved the model's qualitative agreement with observations, though it was still unable to fully capture observed behaviour. Further research is needed to determine the most realistic form of this source term (e.g., exponential or quadratic decay), whether through a physically motivated or a data-driven approach. Future field measurements of in-canopy wind, dew formation, and radiation effects are essential to quantify heat transfer mechanisms in the grass layer and refine the source term. If a generalisable formulation can be established, this could enable new, simplified representations of complex heat transfer within vegetation in land surface models.

Overall, this research represents a step ahead in describing the vegetation layer in land surface heat transfer models by proposing a physically motivated numerical model as an alternative to empirical skin resistance laws. The improved model should remain simple, limiting the number of parameters and vertical layers to incorporate easily into existing forecasting models. By balancing simplicity and accuracy, this model advances the representation of near-surface thermal dynamics in future weather forecasting and climate models.

References

[1] M. Mauder, T. Foken, and J Cuxart. “Surface-energy-balance closure over land: a review”. In: *Boundary-layer meteorology* 177.2 (2020), pp. 395–426.

[2] T. Foken. “50 years of the Monin–Obukhov similarity theory”. In: *Boundary-Layer Meteorology* 119 (2006), pp. 431–447.

[3] J.L. Monteith. “Evaporation and surface temperature”. In: *Quarterly Journal of the Royal Meteorological Society* 107.451 (1981), pp. 1–27.

[4] H.S. Carslaw et al. “Conduction of heat in solids and heat conduction”. In: *Physics Today* 1.7 (1948), pp. 24–24.

[5] K.I. Paul et al. “Soil temperature under forests: a simple model for predicting soil temperature under a range of forest types”. In: *Agricultural and Forest Meteorology* 121.3-4 (2004), pp. 167–182.

[6] G. Hu et al. “New Fourier-series-based analytical solution to the conduction-convection equation to calculate soil temperature, determine soil thermal properties, or estimate water flux”. In: *International Journal of Heat and Mass Transfer* 95 (2016), pp. 815–823.

[7] Pedro Viterbo and Anton CM Beljaars. “An improved land surface parameterization scheme in the ECMWF model and its validation”. In: *Journal of climate* 8.11 (1995), pp. 2716–2748.

[8] B.J.H. Van de Wiel et al. *Amazing grass: a numerical study of atmosphere-grass interactions*. Tech. rep. Copernicus Meetings, 2024.

[9] S.J.A. van der Linden et al. “Heat transfer through grass: a diffusive approach”. In: *Boundary-Layer Meteorology* 184.2 (2022), pp. 251–276.

[10] C.G.B. ter Horst. *Temperature profiles through the soil-vegetation-atmosphere continuum*. TU Delft Repository. 2024.

[11] J.N. Reddy and D.K. Gartling. *The finite element method in heat transfer and fluid dynamics*. CRC press, 2010.

[12] J.N. Reddy. *An Introduction to Continuum Mechanics*. Cambridge University Press, 2013.

[13] R.A. Aulbers. *Modeling Heat Transfer in the Vegetation-Soil Continuum*. TU Delft Repository. 2021.

[14] A.F. Moene and J.C. Van Dam. *Transport in the Atmosphere-Vegetation-Soil Continuum*. Cambridge University Press, 2014.

[15] W.R. Van Wijk and D.A. De Vries. “Periodic temperature variations in a homogeneous soil”. In: *Physics of plant environment* 1 (1963), pp. 103–143.

[16] K. Hanjalic et al. *Analysis and Modelling of Physical Transport Phenomena*. Delft Academic Press/VSSD, 2009.

[17] F.C. Bosveld. *The Cabauw In-situ Observational Program 2000 - Present: Instruments, Calibrations and Set-up*. Tech. rep. TR-384. Royal Netherlands Meteorological Institute (KNMI), 2020.

[18] A.F.G. Jacobs, B.G. Heusinkveld, and S.M. Berkowicz. “Passive dew collection in a grassland area, The Netherlands”. In: *Atmospheric Research* 87.3 (2008), pp. 377–385.

[19] R Horton, P.J. Wierenga, and D.R. Nielsen. “Evaluation of methods for determining the apparent thermal diffusivity of soil near the surface”. In: *Soil Science Society of America Journal* 47.1 (1983), pp. 25–32.

[20] N.H. Abu-Hamdeh. “Thermal Properties of Soils as affected by Density and Water Content”. In: *Biosystems Engineering* 86.1 (2003), pp. 97–102.

[21] H.E.A. van den Akker and R.F. Mudde. *Fysische transportverschijnselen: denken in balansen*. TU Delft Open, 2023.

[22] ECMWF. “IFS Documentation CY48R1 - Part IV: Physical Processes”. In: 4. ECMWF, 2023.

[23] J. Vilà-Guerau De Arellano et al. *Atmospheric boundary layer: Integrating air chemistry and land interactions*. Cambridge University Press, 2015.

[24] B. Schilperoort et al. “A distributed-Temperature-sensing-based soil temperature profiler”. In: *Geoscientific Instrumentation, Methods and Data Systems* 13 (1 Apr. 2024), pp. 85–95. ISSN: 21930864. DOI: 10.5194/gi-13-85-2024.

[25] J. Sauerbier. *Direct Numerical Simulations of the Atmosphere-Grass Boundary Layer*. TU Delft Repository. 2024.

[26] H.A.R. de Bruin and J.N.M. Stricker. “Evaporation of grass under non-restricted soil moisture conditions”. In: *Hydrological Sciences Journal* 45.3 (2000), pp. 391–406.

A

Grass Profiles

Here are the temperature profiles within the grass layer for all June days during the measurement campaign. The in-canopy temperature profiles are given up to a canopy height of $\delta = 0.2$ m. The temperature profiles are shown for each hour. On some days, the temperature profiles for two consecutive hours around midday or midnight lay approximately on top of each other, in line with the assumption for the provisional source term calculation.

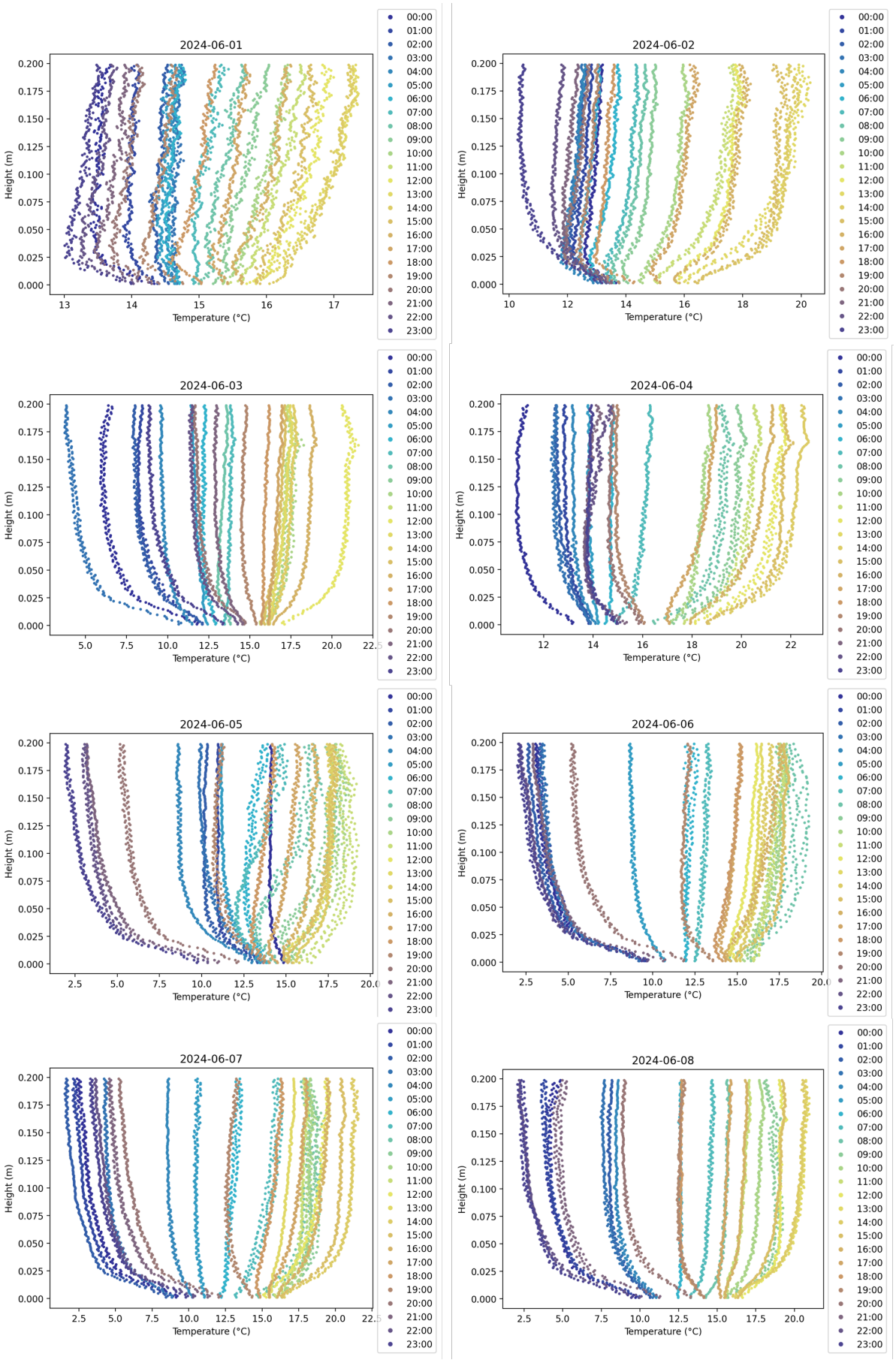

Figure A.1: Daily temperature profiles within the grass layer for June 1^{st} - June 8^{th} 2024.

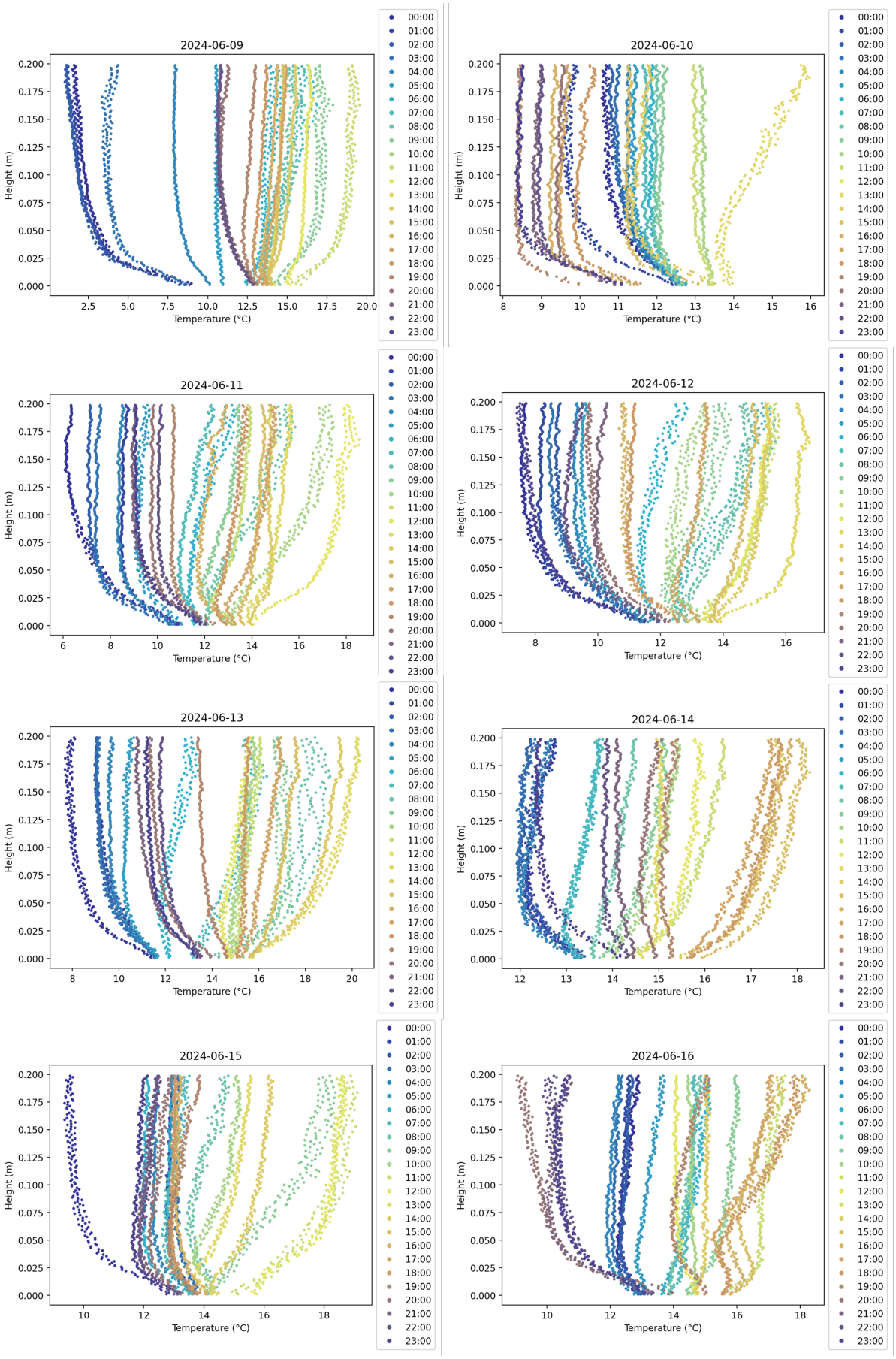

Figure A.2: Daily temperature profiles within the grass layer for June 9^{th} - June 16^{th} 2024.